Critical role of phospholipase A_2 group IID in age-related susceptibility to severe acute respiratory syndrome–CoV infection

Rahul Vijay,[1] Xiaoyang Hua,[2] David K. Meyerholz,[3] Yoshimi Miki,[5] Kei Yamamoto,[5] Michael Gelb,[6,7] Makoto Murakami,[5,8] and Stanley Perlman[1,4]

[1]Interdisciplinary Program in Immunology and [2]Department of Otolaryngology, [3]Department of Pathology, and [4]Department of Microbiology, University of Iowa, Iowa City, IA 52242
[5]Lipid Metabolism Project, Tokyo Metropolitan Institute of Medical Science, Tokyo 156-8506, Japan
[6]Department of Chemistry and [7]Department of Biochemistry, University of Washington, Seattle, WA 98195
[8]Core Research for Evolutional Science and Technology (CREST), Japan Science and Technology Agency, Saitama 332-0012, Japan

Oxidative stress and chronic low-grade inflammation in the lungs are associated with aging and may contribute to age-related immune dysfunction. To maintain lung homeostasis, chronic inflammation is countered by enhanced expression of proresolving/antiinflammatory factors. Here, we show that age-dependent increases of one such factor in the lungs, a phospholipase A_2 (PLA_2) group IID (PLA_2G2D) with antiinflammatory properties, contributed to worse outcomes in mice infected with severe acute respiratory syndrome-coronavirus (SARS-CoV). Strikingly, infection of mice lacking PLA_2G2D expression (*Pla2g2d*$^{-/-}$ mice) converted a uniformly lethal infection to a nonlethal one (>80% survival), subsequent to development of enhanced respiratory DC migration to the draining lymph nodes, augmented antivirus T cell responses, and diminished lung damage. We also observed similar effects in influenza A virus–infected middle-aged *Pla2g2d*$^{-/-}$ mice. Furthermore, oxidative stress, probably via lipid peroxidation, was found to induce PLA_2G2D expression in mice and in human monocyte–derived macrophages. Thus, our results suggest that directed inhibition of a single inducible phospholipase, PLA_2G2D, in the lungs of older patients with severe respiratory infections is potentially an attractive therapeutic intervention to restore immune function.

CORRESPONDENCE
Stanley Perlman:
Stanley-Perlman@uiowa.edu

Abbreviations used: AA, arachidonic acid; AM, alveolar macrophage; CoV, coronavirus; DHA, docosahexaenoic acid; EPA, eicosapentaenoic acid; ESI-MS, electron spray ionization-mass spectrometry; FDR, false discovery rate; HPGDS, hematopoietic prostaglandin D_2 synthase; HPRT, hypoxanthine-guanine phosphoribosyltransferase; IAV, influenza A virus; MDA, malondialdehyde; MDM, monocyte-derived macrophage; MERS, Middle East respiratory syndrome; MFI, mean fluorescent intensity; MLN, mediastinal lymph node; PG, prostaglandin; PLA_2, phospholipase A_2; PLA_2G2D, phospholipase A_2 group II D; PUFA, polyunsaturated fatty acid; SARS, severe acute respiratory syndrome; SPM, specialized proresolving mediators; T reg cells, regulatory T cells; TX, thromboxane.

Aging is associated with a decline in immune function, generally termed immunosenescence (Caruso et al., 2009; Cannizzo et al., 2011), which in turn is often linked to age-related increases in oxidative stress (De La Fuente and Miquel, 2009). Oxidative stress associated with aging has been attributed to the initiation and maintenance of chronic low-grade inflammation ("inflammaging"; Cannizzo et al., 2011). A consequence of immunosenescence is that many viral infections are more severe in aged individuals (Chen and Subbarao, 2007; Assiri et al., 2013; Saad et al., 2014; Alsolamy, 2015). Age-dependent changes in susceptibility are especially striking in patients with the severe acute respiratory syndrome (SARS) or the recently identified Middle East respiratory syndrome (MERS), both caused by coronaviruses (SARS-CoV or MERS-CoV). In the 2002–2003 SARS epidemic, all patients under 24 yr of age survived, whereas 6, 15, and >50% of patients aged 25–44, 45–64, and >65 yr of age, respectively, succumbed to the infection, with many developing acute respiratory distress syndrome (Donnelly et al., 2003; Nicholls et al., 2003; Chen and Subbarao, 2007). This marked age-dependent increase in mortality is also observed in mice and nonhuman primates infected with SARS-CoV (Nagata et al., 2008; Day et al., 2009; Smits et al., 2010; Frieman et al., 2012). For example, 6–10-wk-old C57BL/6 mice are highly resistant to SARS-CoV and remain asymptomatic even in the absence of interferon signaling (Frieman et al., 2010), whereas as mice age from

The Rockefeller University Press $30.00
J. Exp. Med. 2015 Vol. 212 No. 11 1851–1868
www.jem.org/cgi/doi/10.1084/jem.20150632

The Journal of Experimental Medicine

6 wk to 22 mo they become progressively more susceptible to the infection (Zhao et al., 2011).

Mice that succumb to SARS-CoV often develop poor T cell responses (Zhao et al., 2009; Channappanavar et al., 2014). T cell priming to SARS-CoV requires migration of respiratory DCs (rDCs) from the lungs to the mediastinal LNs (MLN). Primed T cells then migrate back to the lungs. We previously showed that rDC migration was greatly decreased in uninfected and SARS-CoV–infected aged compared with young mice. Concomitant with this decreased rDC migratory capacity was an increase in prostaglandin D_2 (PGD_2) in the lungs (Zhao et al., 2011). PGD_2, an eicosanoid with both proinflammatory and antiinflammatory/proresolving properties is a downstream metabolite of arachidonic acid (AA; Samuelsson et al., 1987; Rossi et al., 2000; Straus et al., 2000; Serhan, 2014). PGD_2 binds to two different G-protein–coupled receptors: DP1 expressed on macrophages and DCs (antiinflammatory) and DP2 expressed on Th2 cells (proinflammatory). PGD_2 signaling through the DP1 receptor on respiratory DCs (rDCs) and alveolar macrophages (AMs) in the naive and virus-infected lung, results in, among other effects, decreased CCR7 expression (Hammad et al., 2007; Zhao et al., 2011). This, in turn, results in decreased rDC migration from the lungs to the MLN and poor T cell responses.

To determine the factors behind age-related increases in PGD_2 levels in the lungs, we initially focused on gene expression in $CD11c^+$ cells (AM and rDC) since these cells are key modulators of the immune response in the lungs. We used middle aged (10–13 mo) mice, since these mice, like middle-aged SARS patients, are much more susceptible to the infection than young (6–8 wk) mice, but have not yet developed many of the features of immunosenescence observed in aged (>18 mo animals) and are easier to obtain. Analysis of several genes involved in AA metabolism and oxidative stress in the lungs revealed, most strikingly, that levels of a phospholipase, PLA_2G2D, increased as mice aged. Phospholipases hydrolyze phospholipids to release long-chain fatty acids that are further metabolized sequentially by cyclooxygenases and synthases to yield various lipid mediators. In particular, PLA_2G2D is an enzyme that predominantly contributes to antiinflammatory/proresolving lipid mediator expression (Miki et al., 2013). Therefore, we reasoned that age-related increases in PLA_2G2D could contribute to a delayed immune response and poor outcomes after SARS-CoV infection by up-regulating expression of such lipid mediators. Here, we identified age-related alterations in PLA_2G2D expression in the lungs of uninfected and SARS-CoV–infected mice. Infection of middle-aged mice lacking PLA_2G2D expression (*Pla2g2d*$^{-/-}$) with SARS-CoV resulted in enhanced DC migration to the MLN and antiviral T cell responses, more rapid virus clearance and most remarkably, significantly decreased mortality compared with wild-type (*Pla2g2d*$^{+/+}$) mice.

RESULTS

PLA_2G2D is expressed preferentially in $CD11c^+$ cells in lungs

Because chronic inflammation in the lung increases with aging (MacNee, 2011) and AM and rDC ($CD11c^+$ cells) are critical for maintaining lung homeostasis and for prostaglandin production, we initially examined $CD11c^+$ cells harvested from young and middle-aged mice for global changes in gene expression. Expression levels of 186 genes changed during aging, with many involved in antigen presentation and inflammation (Fig. 1 B and Table S1). Many of these were predicted to contribute to a chronic inflammatory response. However, our previous study showed that levels of a prostaglandin with antiinflammatory properties, PGD_2, were elevated in aged mice (confirmed in Fig. 1 A) and contributed to poor outcomes after SARS-CoV infection (Zhao et al., 2011). Therefore, we next focused on genes involved in the AA pathway, including several phospholipases, cyclooxygenases, and synthases, which could modulate PGD_2 levels in the lungs. Of all the genes in the AA cascade, only levels of secreted phospholipase A_2 group IID (PLA_2G2D) were significantly higher in $CD11c^+$ cells in the lungs of middle-aged compared with young mice (using two-fold differences as a cutoff; Fig. 1, C and D). We confirmed these results by quantitative real-time PCR (qPCR) analyses of $CD11c^+$ cell RNA by separating $CD11c^+$ and $CD11c^-$ cells from the lungs of naive young and middle-aged mice using magnetic beads and quantifying the expression of PLA_2G2D mRNA (Fig. 2 A). We observed 25–30 fold higher expression of PLA_2G2D mRNA in lung $CD11c^+$ compared with $CD11c^-$ cells from middle-aged mice. Comparison of $CD11c^+$ cells from young and middle-aged mice revealed that PLA_2G2D was expressed at levels >50-fold higher in middle-aged mice (Fig. 2 A). Flow cytometric analysis also showed higher expression of PLA_2G2D in $CD11c^+$ compared with $CD11c^-$ cells on a per cell basis in both young and middle-aged mice, as measured by mean fluorescent intensity (MFI; Fig. 2 B). In addition, middle-aged mice harbored a higher frequency of $CD11c^+$ cells expressing PLA_2G2D compared with young mice (Fig. 2 C).

Together, these results indicate that PLA_2G2D levels are highly increased in the lungs of middle-aged mice and that $CD11c^+$ cells are the major source for its production. However, regulatory T cells (T reg cells; $CD4^+FoxP3^+$) have been implicated as a source for PLA_2G2D in previous studies (von Allmen et al., 2009) and lungs of uninfected middle-aged mice harbor higher frequency and number of T reg cells compared with young mice (Fig. 2 D). To address whether T reg cells are an additional source for PLA_2G2D, we depleted CD4 T cells, which includes T reg cells, from middle-aged mice and analyzed lungs for expression of PLA_2G2D. We observed no changes in the mRNA expression of PLA_2G2D after CD4 T cell depletion (Fig. 2 E), suggesting that CD4 T cells, including T reg cells, are not a major source of PLA_2G2D in the lungs.

Because $CD11c^+$ cells comprise only a minority of the total cells in the lungs, expression of PLA_2G2D by these cells could make a relatively small contribution to its total production. However, this was not the case because levels of PLA_2G2D were significantly higher in unfractionated lung mRNA from middle-aged compared with young mice. Notably, PLA_2G2D levels were even higher in samples obtained from aged (22 mo) mice (Fig. 3 A). Assessment of other genes in the AA cascade

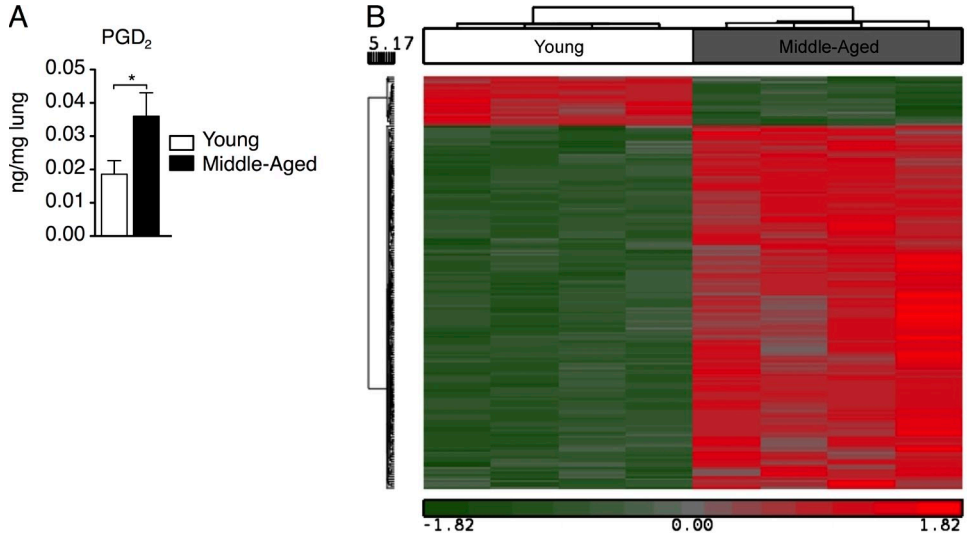

D

Probeset ID	SYMBOL	stepup(p-value)	Ratio	Fold-Change	Mean Expression (log2) Middle Aged	Young
PLA2G2D	Pla2g2d	0.0415145	2.31163	2.31163	5.6162125	4.4073025
CBR3	Cbr3	0.00805233	1.7952	1.7952	8.1723275	7.3281825
PTGIS	Ptgis	0.064817	1.70723	1.70723	5.638805	4.8671475
PLA2G12A	Pla2g12a	0.0111315	1.59677	1.59677	7.4231375	6.747985
PLA2G4A	Pla2g4a	0.247936	1.53182	1.53182	3.8876275	3.2723775
PLA2G2A	Pla2g2a	0.495766	1.31942	1.31942	3.91912	3.5192175
PTGES3	Ptges3	0.137871	1.27955	1.27955	8.0436575	7.688025
PLA2G5	Pla2g5	0.367134	1.21707	1.21707	4.6020825	4.318665
PLA2G3	Pla2g3	0.631922	1.16817	1.16817	3.9919875	3.7677325
PTGES	Ptges	0.525022	1.16001	1.16001	5.325155	5.111015
PLA2G4C	Pla2g4c	0.560696	1.1019	1.1019	3.8501325	3.71014
GPX8	Gpx8	0.782737	1.07516	1.07516	5.1037425	4.99919
PLA2G4B	Pla2g4b	0.856843	1.0637	1.0637	5.1087825	5.019695
GGT5	Ggt5	0.817934	1.05489	1.05489	4.389635	4.31255
PLA2G16	Pla2g16	0.909381	1.04922	1.04922	4.125625	4.0563075
PLB1	Plb1	0.912437	1.04417	1.04417	3.9190325	3.8566825
PTGDS	Ptgds	0.952438	1.02085	1.02085	4.42494	4.3951625
CBR1	Cbr1	0.921324	1.01781	1.01781	7.779575	7.7541075
PLA2G4D	Pla2g4d	0.94783	1.01629	1.01629	4.2118325	4.1885225
ALOX12E	Alox12e	0.997814	1.00055	1.00055	4.3917125	4.3909175
GGT1	Ggt1	0.952675	0.9826	-1.01771	4.7225825	4.7479075
ALOX5	Alox5	0.867794	0.96982	-1.03112	10.0420375	10.0862675
GPX1	Gpx1	0.243231	0.961051	-1.04053	13.2276	13.284925
PLA2G6	Pla2g6	0.854288	0.958058	-1.04378	4.994875	5.05669
PLA2G4F	Pla2g4f	0.856843	0.949429	-1.05327	4.8956475	4.9705175
PLA2G2E	Pla2g2e	0.710786	0.937661	-1.06648	4.385845	4.4787025
ALOX12B	Alox12b	0.802111	0.932536	-1.07234	4.347775	4.4485425
ALOX15	Alox15	0.621666	0.92646	-1.07938	3.9663725	4.07657
ALOX8	Alox8	0.867116	0.924299	-1.0819	4.2357025	4.349275
PLA2G2F	Pla2g2f	0.681678	0.909199	-1.09987	4.4695075	4.6068375
PLA2G12B	Pla2g12b	0.686351	0.903086	-1.10731	3.9189825	4.06605
PLA2G10	Pla2g10	0.821217	0.892905	-1.11994	3.92042	4.08384
PTGES2	Ptges2	0.602633	0.884756	-1.13025	6.334155	6.5108025
PTGDS2	Ptgds2	0.528266	0.878009	-1.13894	4.7338675	4.9215575
GPX7	Gpx7	0.336866	0.860095	-1.16266	4.5230425	4.7404725
PLA2G4E	Pla2g4e	0.584944	0.858	-1.1655	4.5343975	4.755345
GPX5	Gpx5	0.397071	0.849782	-1.17677	3.867675	4.10251
PTGS2	Ptgs2	0.349433	0.84805	-1.17918	3.8629025	4.1006825
GPX6	Gpx6	0.641039	0.836776	-1.19506	4.206385	4.4634725
ALOX12	Alox12	0.672123	0.810814	-1.23333	5.397485	5.7000425
GPX2	Gpx2	0.5717	0.808478	-1.23689	4.2441	4.5508175
PLA2G1B	Pla2g1b	0.452632	0.758762	-1.31794	3.758975	4.1572575
PLA2G2C	Pla2g2c	0.408596	0.752502	-1.3289	3.9645575	4.3747925
CBR2	Cbr2	0.249775	0.71111	-1.40625	7.96609	8.4579475
LTC4S	Ltc4s	0.00665231	0.665755	-1.50206	11.042625	11.62955

Figure 1. Differential gene expression in pulmonary CD11c$^+$ cells from middle-aged and young mice. (A) Lungs from naive young (6–8 wk) and middle-aged (10–13 mo) C57BL/6 mice were analyzed for PGD_2 expression by LC/MS analysis. Mean ± SEM; two independent experiments, five mice/group. *, $P < 0.05$, unpaired Student's *t* test. (B) Heat map depicting differential gene expression in pulmonary CD11c$^+$ cells from young and middle-aged mice. (C and D) Heat map and table depicting differential expression of genes involved in AA metabolism in pulmonary CD11c$^+$ cells. Table shows step-up p-value (after correcting for multiple comparisons), fold change, and mean expression values of different genes ($n = 4$/group).

generally confirmed the microarray results shown in Fig. 1 C and showed that there were no differences in the levels of expression of the cyclooxygenase enzymes COX_1 and COX_2 or other PLA_2s (PLA_2G2E, PLA_2G3, PLA_2G4, PLA_2G5, and PLA_2G10) as mice aged (Fig. 3, B and C). One exception is that there were significantly higher mRNA levels of hematopoietic PGD_2 synthase (HPGDS), which is important for PGD_2 production and could contribute to elevated PGD_2 levels in the lungs of middle-aged compared with young mice (Fig. 3 C; Murata et al., 2013).

Because robust expression of PLA_2G2D in lymphoid tissue CD11c$^+$ cells was previously reported (Miki et al., 2013), we

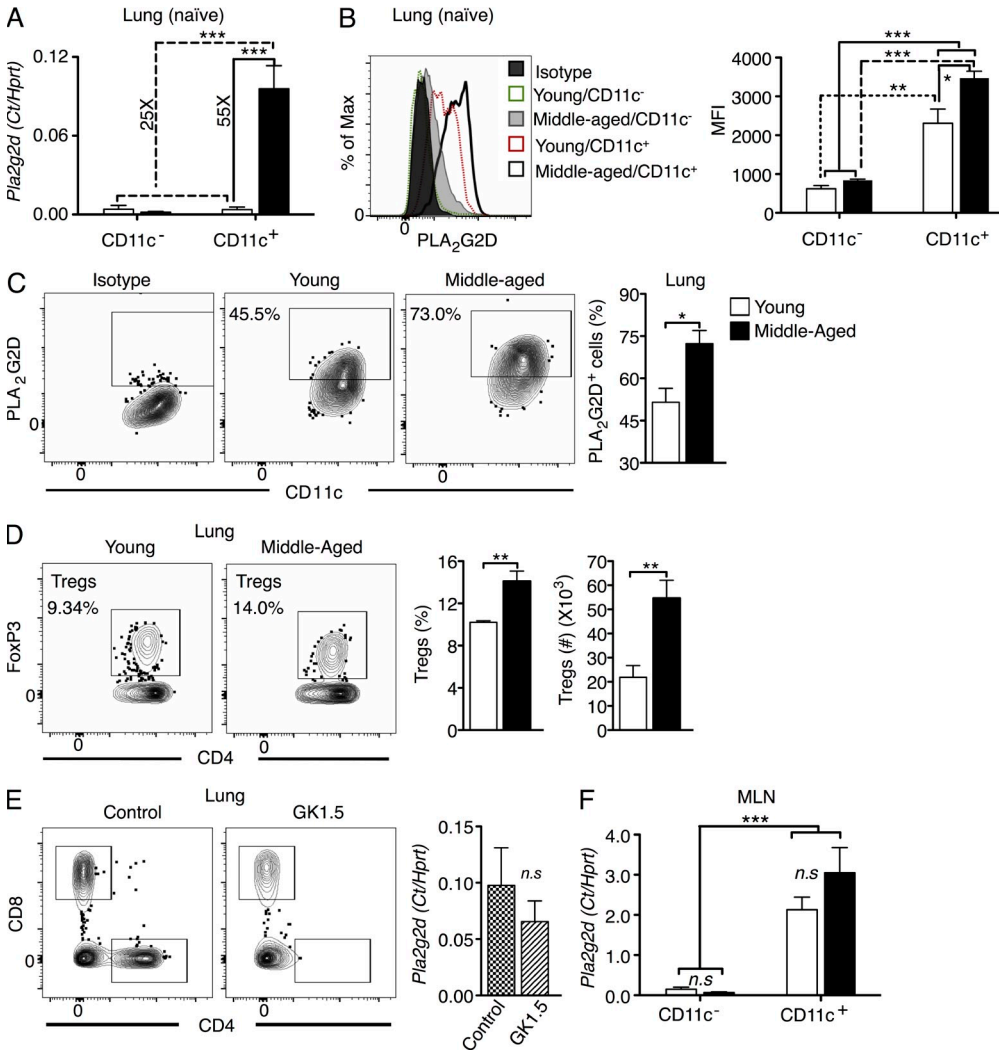

Figure 2. PLA_2G2D expression in CD11c cells in the lungs and MLN of middle-aged mice. (A) PLA_2G2D mRNA levels in $CD11c^-$ and $CD11c^+$ cells from the lungs of young and middle-aged mice. $CD11c^+$ and $CD11c^-$ cells were prepared from the lungs of naive young or middle-aged mice using CD11c magnetic beads and analyzed for PLA_2G2D mRNA levels using qPCR. Mean ± SEM; two independent experiments, eight mice/group. ***, $P < 0.001$, unpaired Student's *t* test. (B) Representative histograms comparing the mean fluorescent intensity of PLA_2G2D expression in $CD11c^-$ and $CD11c^+$ cells (gated on $CD45^+$ cells) of young and middle aged mice (left). Summary data are shown on right. Single-cell suspension from the lungs of naive young and middle-aged mice were stained for PLA_2G2D and analyzed by flow cytometry as described in the Materials and methods. Mean ± SEM; three independent experiments, four mice/group. *, $P < 0.05$; **, $P < 0.01$; ***, $P < 0.001$, unpaired Student's *t* test. (C) Frequency of $CD11c^+$ cells (gated on $CD45^+$) expressing PLA_2G2D in the lungs of naive young and middle aged mice. The boxed area in the flow cytometry plots indicates cell populations staining positive for PLA_2G2D. Mean ± SEM; three independent experiments, four mice/group. *, $P < 0.05$, unpaired Student's *t* test. (D) Frequency and total number of $FoxP3^+$ $CD4^+$ T reg cells (gated on $CD3^+CD8^-$). Mean ± SEM; two independent experiments, four mice/group. **, $P < 0.01$, unpaired Student's *t* test. (E) PLA_2G2D expression in absence of CD4 T cells. (left) Extent of depletion of CD4 T cells on day 4 after GK1.5 treatment; (right) mRNA expression of PLA_2G2D in the lungs of treated (GK1.5) and control groups. CD4 T cells were depleted using mAb GK1.5, delivered i.p. at 0.5 mg/mouse on day 0 and 2. 2 d later, lungs were harvested into TRIzol for quantifying PLA_2G2D RNA levels. PBS was administered to control mice. Mean ± SEM; two independent experiments, four mice/group. n.s., not significant, unpaired Student's *t* test. (F) $CD11c^+$ and $CD11c^-$ cells were harvested from the MLN of naive young and middle-aged mice. PLA_2G2D mRNA levels were determined using qPCR. Mean ± SEM; two independent experiments, four mice/group. n.s., not significant; ***, $P < 0.001$, unpaired Student's *t* test.

determined whether its levels increased with age in the MLN. As expected, we observed higher expression of PLA_2G2D in $CD11c^+$ compared with $CD11c^-$ cells in the MLN (Fig. 2 F). However, unlike in the lungs, there were no age-dependent differences in PLA_2G2D mRNA expression in MLN $CD11c^+$ cells between young and middle-aged naive mice. Collectively, these results indicate that PLA_2G2D is nearly exclusively expressed in $CD11c^+$ cells in both lymphoid tissue and lungs and that age-related differences in its expression are confined to the lungs.

PLA_2G2D-dependent alteration in pulmonary lipid profile

PLA_2G2D has been previously described as a proresolving phospholipase acting upstream in the AA-cascade (Miki et al., 2013).

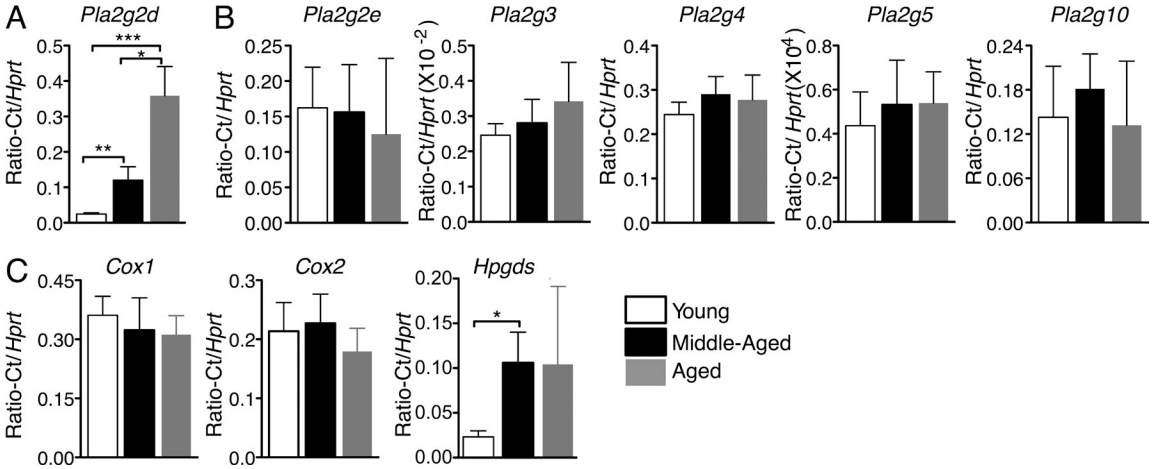

Figure 3. Age-dependent changes in the AA cascade in the lung. Young, middle-aged, and aged (22 mo) C57BL/6 mice were analyzed for mRNA expression levels of several enzymes in the AA pathway. (A) PLA_2G2D mRNA levels in the lungs. Mean ± SEM; two independent experiments, four mice/group. *, $P < 0.05$; **, $P < 0.01$; ***, $P < 0.001$, unpaired Student's *t* test. (B) mRNA levels of other phospholipases. Mean ± SEM; two independent experiments, four mice/group, unpaired Student's *t* test. (C) cyclooxygenases and hematopoietic PGD2 synthase (HPGDS) in the lungs. Mean ± SEM; two independent experiments, four mice/group. *, $P < 0.05$, unpaired Student's *t* test. All gene expression data are normalized to *Hprt* expression.

Hence, we reasoned that higher expression levels of PLA_2G2D in the lungs of middle-aged mice would result in perturbation in lipid metabolism and that lipid mediators with proresolving functions, other than PGD_2, would also be produced at higher levels. To investigate this possibility, we performed electrospray ionization mass spectrometry (ESI-MS) to determine the levels of free polyunsaturated fatty acids (PUFAs), as well as their oxygenated metabolites, including PGD_2, in the lungs of naive young and middle-aged mice (Fig. 4, B–D). Initial analyses revealed altered profiles of lipid mediators with both pro- and antiinflammatory function in the lungs of middle-aged relative to young mice. Levels of free PUFA such as AA (ω6) and docosahexaenoic acid (DHA; ω3) were not significantly different between the groups, whereas the level of eicosapentaenoic acid (EPA) was higher in middle-aged mice relative to young mice (Fig. 4 B). AA metabolites with antiinflammatory (PGE_2 and PGD_2) and proinflammatory properties (PGF2α and Thromboxane [TX] B_2 [a TXA_2 metabolite]) were produced at higher levels in the lungs of middle-aged mice compared with young mice, but levels of 6-keto-PGF1α (a PGI_2 metabolite) did not differ between the groups (Fig. 4, C and D).

PLA_2G2D is one of many PLA_2 expressed in the lungs, but is the only one that was up-regulated as mice aged, as shown above. Therefore, we next assessed whether PLA_2G2D mediated the perturbation in pulmonary lipid profile in middle-aged mice using *Pla2g2d*$^{-/-}$ and *Pla2g2d*$^{+/+}$ mice (Miki et al., 2013). Lipid profiling of the lungs of middle-aged *Pla2g2d*$^{-/-}$ and *Pla2g2d*$^{+/+}$ mice revealed an important role for PLA_2G2D in the levels of most lipids examined (Fig. 4, H–J). Of note, these changes were not observed when young *Pla2g2d*$^{-/-}$ and *Pla2g2d*$^{+/+}$ mice were compared (Fig. 4, E–G). AA was produced at lower levels in *Pla2g2d*$^{-/-}$ relative to *Pla2g2d*$^{+/+}$ middle-aged mice (Fig. 4 H), suggesting that phospholipase activity required to release AA was at least partly dependent on PLA_2G2D. Levels of 6ketoPGF1α, TXB_2, PGF2α, PGD_2, and PGE_2 were also higher in the lungs of *Pla2g2d*$^{+/+}$ compared with *Pla2g2d*$^{-/-}$ mice (Fig. 4, I and J), suggesting that differences in AA levels resulted in differences in the levels of its downstream metabolites, some of which have antiinflammatory function (PGD_2 and PGE_2; Vancheri et al., 2004; Kalinski, 2012; Murata et al., 2013). The results also identify PLA_2G2D-dependent pools of two other PUFA, DHA, and EPA in the lungs. DHA and EPA are further metabolized largely into proresolving mediators, such as resolvin D1, protectin D1, and resolvin E1 among others (Arita et al., 2005; Rogerio et al., 2012).

PLA_2G2D dependent up-regulation of PGD_2 and other antiinflammatory lipid mediators in the lungs of SARS-CoV–infected middle-aged mice

Having established that both proinflammatory and antiinflammatory/proresolving lipid mediators are up-regulated in the uninfected lungs of middle-aged mice, we next determined whether levels of these mediators were further perturbed in the context of infection. We initially analyzed mice infected with SARS-CoV because middle-aged but not young C57BL/6 mice succumb to infection with this virus, mimicking the human disease (Fig. 5 A; Frieman et al., 2012; Zhao et al., 2012). Because mortality in middle-aged mice begins at 4 d after SARS-CoV infection, we investigated whether levels of lipid mediators, including PGD_2, changed at this time. Expression levels of PLA_2G2D increased in both young and middle-aged mice after infection (Fig. 5 B). Further, pulmonary lipid profiling on day 4 postinfection (p.i.) revealed significant increases in lung levels of free PUFAs such as AA, EPA, and DHA in middle-aged mice but less so in young mice

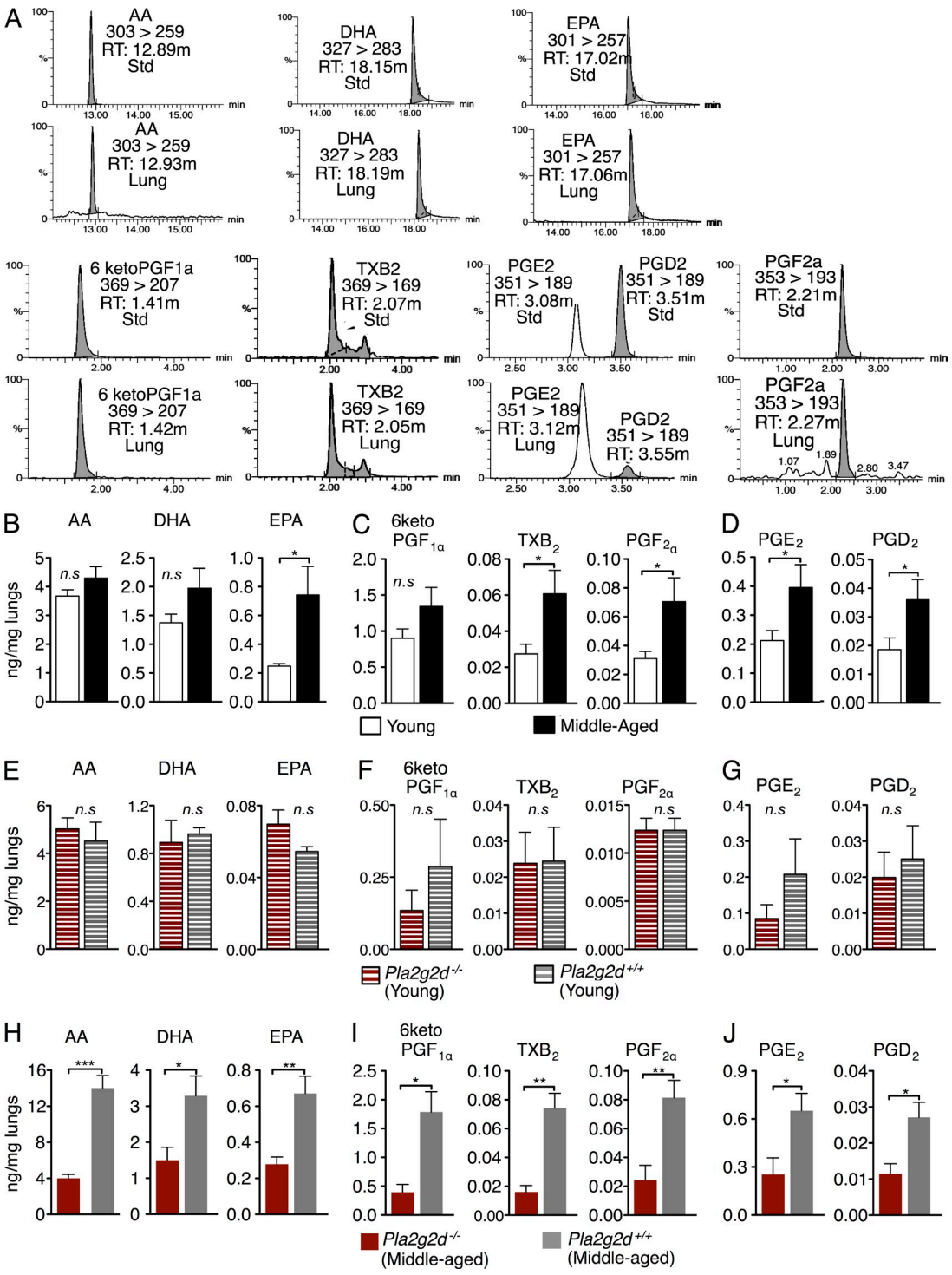

Figure 4. PLA_2G2D-dependent alteration of lipid profile in the lungs. Naive young and middle-aged C57BL/6 mice (B–D) and *Pla2g2d*$^{-/-}$ *and Pla2g2d*$^{+/+}$ mice (E–J) were analyzed for pulmonary lipids using ESI-MS as described in Materials and methods. (A) The elution of different endogenous lipids with respect to exogenous standards (SD) is indicated. Retention times and parent m/z to daughter m/s transition are also shown. Levels of (B) free PUFAs, AA, DHA and EPA. Mean ± SEM; three independent experiments, four mice/group. n.s., not significant; *, $P < 0.05$, unpaired Student's *t* test. (C) 6ketoPGF$_{1\alpha}$, TXB_2, and PGF$_{2\alpha}$. Mean ± SEM; three independent experiments, four mice/group. n.s., not significant; *, $P < 0.05$, unpaired Student's *t* test. (D) PGE_2 and PGD_2 in lungs of young and middle-aged C57BL/6 mice are shown. Mean ± SEM; three independent experiments, four mice/group. n.s., not significant; *, $P < 0.05$, unpaired Student's *t* test. (E) Levels of free PUFAs. Mean ± SEM; two independent experiments, four mice/group, unpaired Student's *t* test. (F) 6-keto-PGF$_{1\alpha}$, TXB_2, and PGF$_{2\alpha}$. Mean ± SEM; two independent experiments, four mice/group, unpaired Student's *t* test. (G) PGE_2 and PGD_2 in lungs of young *Pla2g2d*$^{-/-}$ *and Pla2g2d*$^{+/+}$ mice. Mean ± SEM; two independent experiments, four mice/group, unpaired Student's *t* test. (H) Levels of

(Fig. 5 C). Levels of lipid mediators with proinflammatory activity, 6ketoPGF1α, TXB_2, and PGF2α, increased in the lungs of young but not middle-aged mice after SARS-CoV infection (Fig. 5 D). In contrast, levels of PGE_2 and PGD_2, both of which have antiinflammatory activity in the lungs, increased in both young and middle-aged mice after infection (Fig. 5 E).

To determine whether the inducible pool of these lipids is dependent on PLA_2G2D, we determined the lung lipid profile in SARS-CoV–infected middle-aged *Pla2g2d*$^{-/-}$ and *Pla2g2d*$^{+/+}$ mice. Whereas levels of free PUFAs, AA, DHA, and EPA increased in the lungs of both groups of mice during infection, *Pla2g2d*$^{+/+}$ mice harbored higher levels of all three fatty acids at all times examined (Fig. 5 F), indicating that the inducible pool of each of these fatty acids was at least partly mediated by PLA_2G2D. We did not observe an infection-dependent increase in the levels of 6-keto-PGF1α, TXB_2, or PGF2α in either group of mice, although levels remained higher in *Pla2g2d*$^{+/+}$ mice relative to *Pla2g2d*$^{-/-}$ mice on day 4 p.i. (Figs. 4 I and 5 G). PGE_2 and PGD_2 levels increased only in *Pla2g2d*$^{+/+}$ mice after infection (Fig. 5 H). These results indicate multifactorial regulation of the inducible AA cascade with basal levels of all lipid mediators were maintained at least partly by PLA_2G2D, whereas increases in PGE_2 and PGD_2 levels observed after SARS-CoV infection in the lungs were largely dependent on PLA_2G2D. These data also agree with published studies showing that induction of PLA_2G2D generated pools of proresolving but not proinflammatory mediators in the lung and skin in the context of allergic disease (Nagao et al., 2003; Kunikata et al., 2005; Liu et al., 2012; Miki et al., 2013).

PLA_2G2D plays a minor role in innate immune functions in the lungs of middle-aged mice

The preferential induction of antiinflammatory lipid mediators in *Pla2g2d*$^{-/-}$ mice could contribute to less efficient activation of the innate and adaptive immune responses. To address this possibility, we initially analyzed the activation status and function of lung CD11c$^+$ cells harvested from middle-aged and young mice at day 1 after SARS-CoV infection. Cells from middle-aged mice expressed significantly higher levels of maturation markers (CD40, CD80, and MHCII) and expressed higher levels of TNF in the absence of ex vivo stimulation (basal levels) compared with young mice (Fig. 6, A and B [RP10]). However upon TLR stimulation with LPS or poly I:C, similar frequencies of CD11c$^+$ cells from both young and middle-aged mice produced TNF, although the total number of TNF-producing cells was higher in middle-aged mice (Fig. 6 B, middle and bottom).

To investigate the role of PLA_2G2D in this enhanced CD11c$^+$ cell activation in middle-aged mice, we measured CD40, CD80, and MHCII levels on lung CD11c$^+$ cells harvested from infected middle-aged *Pla2g2d*$^{+/+}$ and *Pla2g2d*$^{-/-}$ mice and also quantified TNF expression after TLR stimulation. PLA_2G2D was required for MHCII but not CD40 or CD80 expression on lung CD11c$^+$ cells in middle-aged mice, and for increased frequency but not number of cells expressing TNF in the absence of any direct ex vivo stimulation with TLR ligands. CD11c$^+$ cells from both *Pla2g2d*$^{+/+}$ and *Pla2g2d*$^{-/-}$ mouse lungs were able to express equivalent amounts of TNF after direct ex vivo stimulation (Fig. 6, C and D). Thus, these results indicate that CD11c$^+$ cells from infected middle-aged *Pla2g2d*$^{+/+}$ mice were more highly activated in vivo compared with young C57BL/6 mice, but that PLA_2G2D has a relatively minor role in age-dependent differences in CD11c$^+$ cell maturation and function.

These results show that the major effect of PLA_2G2D is to increase levels of antiinflammatory lipid mediators, but changes in expression may also have indirect or direct effects on levels of cytokines and other inflammatory mediators. However, we observed no differences in expression of several proinflammatory molecules or IL-10, a cytokine with antiinflammatory properties, in the lungs of *Pla2g2d*$^{+/+}$ and *Pla2g2d*$^{-/-}$ mice at days 1 or 4 p.i. (Fig. 6 E). Thus, PLA_2G2D has only small effects on general innate immune function in middle-aged mice and its absence largely affects only the expression of lipid mediators.

Absence of PLA_2G2D enhances rDC migration to draining lymph nodes

PGD_2 inhibits the migration of airway DCs from lungs to the MLN in middle-aged naive and SARS-CoV–infected mice (Hammad et al., 2003; Zhao et al., 2011) and while levels of PGD_2 decreased in *Pla2g2d*$^{-/-}$ mice, it was not known a priori whether this decrease was sufficient to correct the defect in rDC migration. To determine whether this was the case, we first instilled OVA-FITC intranasally (i.n.) into uninfected middle-aged *Pla2g2d*$^{+/+}$ and *Pla2g2d*$^{-/-}$ mice and analyzing MLN 18 h later for OVA-FITC$^+$ rDCs, indicative of migration from the lungs. We observed that a higher frequency and number of rDCs migrated to the MLN in the absence of PLA_2G2D (Fig. 6 F). We next investigated whether rDC migration was augmented in mice infected with SARS-CoV by instilling CFSE i.n. into middle-aged *Pla2g2d*$^{+/+}$ and *Pla2g2d*$^{-/-}$ mice 6 h before infection. 18 h p.i. MLN were harvested and analyzed for the frequency of rDCs that migrated from lungs (CD11c$^+$MHCII$^+$CFSE$^+$ population). *Pla2g2d*$^{-/-}$ mice harbored a higher frequency and number of CFSE$^+$ rDCs in MLN compared with *Pla2g2d* $^{+/+}$ mice (Fig. 6 G). Migration of DCs from the site of infection to the MLN is mediated by chemokine receptor CCR7 binding to CCL19/21 (Hamilton-Easton and Eichelberger, 1995; Fainaru et al., 2005) and DCs

free PUFAs. Mean ± SEM; two independent experiments, four mice/group, unpaired Student's *t* test. (I) 6-keto-$PGF_{1\alpha}$, TXB_2, and $PGF_{2\alpha}$. Mean ± SEM; two independent experiments, four mice/group, unpaired Student's *t* test. (J) PGE_2 and PGD_2 in lungs of middle-aged *Pla2g2d*$^{-/-}$ and *Pla2g2d*$^{+/+}$ mice. Mean ± SEM; two independent experiments, four mice/group. *, $P < 0.05$; **, $P < 0.01$; ***, $P < 0.001$, unpaired Student's *t* test.

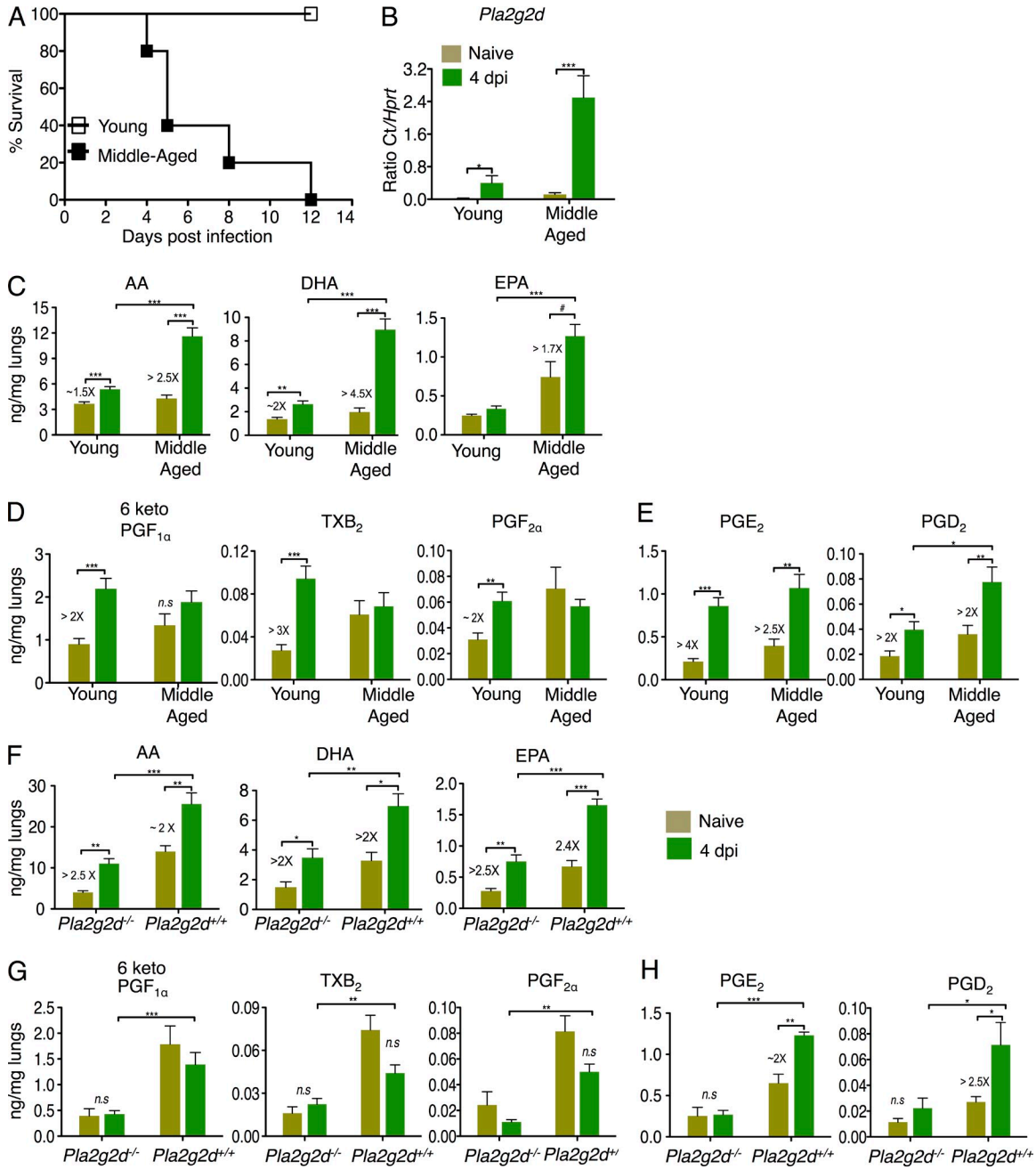

Figure 5. PLA_2G2D-dependent up-regulation of PGD2 and other lipid mediators after SARS-CoV infection. (A) Survival of young and middle-aged C57BL/6 mice after i.n. challenge with 10^4 PFU of SARS-CoV (two independent experiments, five mice/group). Naive or infected young and middle aged C57BL/6 mice (B–E) or middle-aged *Pla2g2d*$^{-/-}$ *and Pla2g2d*$^{+/+}$ mice (F–H) were analyzed for mRNA expression levels of PLA_2G2D in and lipid expression in the lungs using qPCR and ESI-MS, respectively, as described in Materials and methods. (B) mRNA levels of PLA_2G2D in the lungs of young and middle-aged mice before (light green) and 4 d p.i. (dark green), expressed relative to *Hprt*. Mean ± SEM; two independent experiments, four mice/group. *, $P < 0.05$; ***, $P < 0.001$, unpaired Student's *t* test. Comparison of levels in the lungs of young and middle-aged mice of (C) free PUFAs, AA, DHA, and EPA. Mean ± SEM; two independent experiments, four mice/group. #, $P = 0.07$; **, $P < 0.01$; ***, $P < 0.001$, unpaired Student's *t* test. (D) $6ketoPGF_{1\alpha}$, TXB_2, and $PGF_{2\alpha}$. Mean ± SEM; three independent experiments, four mice/group. **, $P < 0.01$; ***, $P < 0.001$, unpaired Student's *t* test. (E) PGE_2 and PGD_2 before and 4 d p.i. Mean ± SEM; three independent experiments, four mice/group. *, $P < 0.05$; **, $P < 0.05$; ***, $P < 0.001$, unpaired Student's *t* test. Comparison of levels in the lungs of middle-aged *Pla2g2d*$^{-/-}$ *and Pla2g2d*$^{+/+}$ mice of (F) free PUFAs. Mean ± SEM; two independent experiments, five mice/group. n.s., not significant; *, $P < 0.05$; **, $P < 0.01$; ***, $P < 0.001$ (unpaired Student's *t* test). (G) $6ketoPGF_{1\alpha}$, TXB_2, and $PGF_{2\alpha}$. Mean ± SEM; two independent experiments, five mice/group. n.s., not significant; **, $P < 0.01$; ***, $P < 0.001$, unpaired Student's *t* test. (H) PGE_2 and PGD_2 before and 4 d p.i. Mean ± SEM; two independent experiments, five mice/group. n.s., not significant; *, $P < 0.05$; **, $P < 0.01$; ***, $P < 0.001$ (unpaired Student's *t* test). All lipid concentrations are expressed as nanogram/milligram lung tissue.

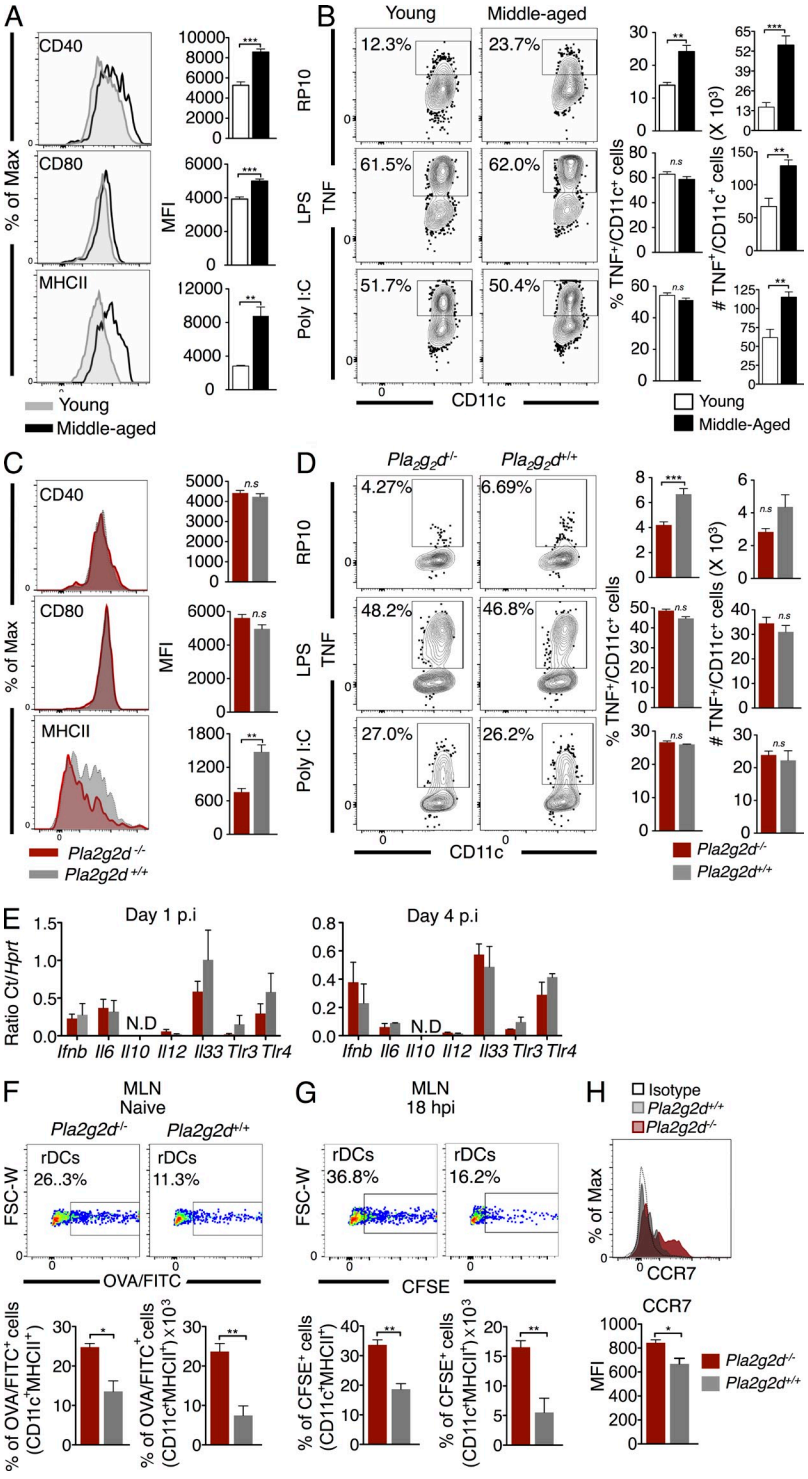

Figure 6. rDC activation and function in young and aged mice or *Pla2g2d*$^{-/-}$ and *Pla2g2d*$^{+/+}$ mice. Young and middle-aged C57BL/6 mice (A and B) or middle-aged *Pla2g2d*$^{-/-}$ or *Pla2g2d*$^{+/+}$ mice (C–E, G, and H) were infected with 10^4 PFU SARS-CoV and analyzed for activation status, and functionality of pulmonary CD11c$^+$ cells after TLR stimulation. (A) Expression of activation markers CD40 (top row), CD80 (middle row), and MHCII (bottom row) on lung CD11c$^+$ from young and middle-aged C57BL/6 mice. Representative histograms and summary bar graphs are shown. Mean ± SEM; two independent experiments, four mice/group. **, $P < 0.01$; ***, $P < 0.001$, unpaired Student's *t* test. (B) TNF production after vehicle (RP10, top row), LPS (middle row), or poly I:C (bottom row) stimulation is shown. Mean ± SEM; two independent experiments, four mice/group. n.s., not significant. **, $P < 0.01$; ***, $P < 0.001$, unpaired Student's *t* test. (C) Expression of activation markers CD40 (top row), CD80 (middle row), and MHCII (bottom row) on lung CD11c$^+$ from middle-aged *Pla2g2d*$^{-/-}$ or *Pla2g2d*$^{+/+}$ mice. Representative histograms and summary bar graphs are shown. Mean ± SEM; two independent experiments, four mice/group. n.s., not significant; **, $P < 0.01$, unpaired Student's *t* test. (D) TNF production after vehicle (RP10, top row), LPS (middle row), or poly I:C (bottom row) stimulation. Mean ± SEM; two independent experiments, four mice/group. n.s., not significant; ***, $P < 0.001$, unpaired Student's *t* test. (E) mRNA expression levels of proinflammatory cytokines, TLR3 and TLR4 in the lungs of middle-aged *Pla2g2d*$^{-/-}$ or *Pla2g2d*$^{+/+}$ mice on day 1 (left panel) and day 4 p.i. (right panel) Mean ± SEM; two independent experiments, four mice/group, unpaired Student's *t* test. N.D., not detected. (F) Naive middle-aged *Pla2g2d*$^{-/-}$ or *Pla2g2d*$^{+/+}$ mice were intranasally inoculated with 200 µg/75 µl OVA-FITC. 18 h later, MLNs were harvested and analyzed. Mean ± SEM; two independent experiments, four mice/group. *, $P < 0.05$; **, $P < 0.01$, unpaired Student's *t* test. (G) Frequency and number of airway DCs (CD11c$^+$MHCII$^+$CFSE$^+$) that migrated from the lung to MLN, 18 h after SARS-CoV infection. 50 µl of 8 µM CFSE was instilled intranasally 6 h before infection. At 18 h p.i., MLNs were harvested and analyzed. Gated on CD45$^+$CD11c$^+$MHCII$^+$CFSE$^+$ cells Mean ± SEM; three independent experiments, four mice/group. **, $P < 0.01$, unpaired Student's *t* test. (H) MFI of CCR7 expression on rDCs in lungs (gated on CD45$^+$CD11c$^+$MHCII$^+$CFSE$^+$) 18 h p.i. Mean ± SEM; two independent experiments, four mice/group. *, $P < 0.05$, unpaired Student's *t* test.

differentiated in the presence of PGD_2 express lower levels of CCR7 (Gosset et al., 2005; Zhao et al., 2011). Consistent with higher expression of PLA_2G2D and PGD_2 in the lungs, *Pla2g2d*$^{-/-}$ rDCs expressed higher CCR7 surface levels than *Pla2g2d*$^{+/+}$ rDCs, contributing to enhanced rDC migration to the draining lymph nodes in uninfected and SARS-CoV–infected mice (Fig. 6 H).

Enhanced T cell responses and increased survival in SARS-CoV–infected *Pla2g2d*$^{-/-}$ mice

Having demonstrated superior migration of rDCs to the MLN in *Pla2g2d*$^{-/-}$ mice, we next assessed whether this translated into more robust virus-specific CD4 and CD8 T cell responses in infected lungs (Fig. 7). We addressed this possibility by examining the CD4 and CD8 T cell response in SARS-CoV–infected

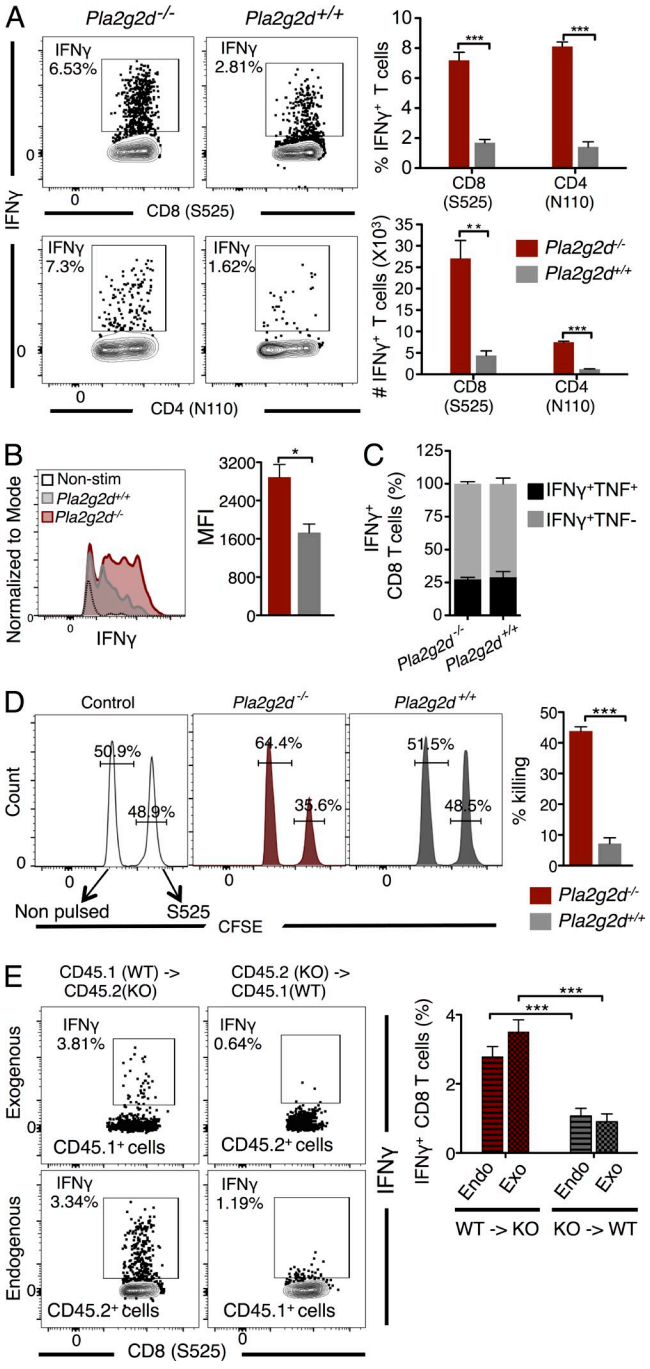

Figure 7. PLA_2G2D dampening of the anti–SARS-CoV T cell response. SARS-CoV–infected middle-aged *Pla2g2d*$^{-/-}$ *or Pla2g2d*$^{+/+}$ mice were analyzed for quantity and quality T cell responses in the lungs, as described in Materials and methods. (A) Representative flow plots showing frequency of virus-specific CD8 (S525 specific) and CD4 (N110 specific) T cell responses on day 6 after infection with 10^4 PFU SARS-CoV. Summary data for frequency and total number of virus-specific T cells are shown in the bar graphs. Mean ± SEM; of two independent experiments, five mice/group. **, $P < 0.01$; ***, $P < 0.001$, unpaired Student's *t* test. (B) Amount of IFN-γ produced on a per cell basis by CD8 T cells is depicted as MFI. Mean ± SEM; of two independent experiments, five mice/group. *, $P < 0.05$, unpaired Student's *t* test. (C) Representative data showing proportion of virus-specific T cells in the lungs expressing IFN-γ alone or IFN-γ and TNF. Mean ± SEM; of two independent experiments, five mice/group, unpaired Student's *t* test. (D) In vivo cytotoxicity was assessed on day 6 p.i and the percentage killing was determined as described in Materials and methods. Data show killing of target cells in the lungs of *Pla2g2d*$^{-/-}$ *or Pla2g2d*$^{+/+}$ mice. Mean ± SEM; three independent experiments, five mice/group. ***, $P < 0.001$ (unpaired Student's *t* test). (E) Representative flow plots of virus-specific T cell responses in recipient *Pla2g2d*$^{-/-}$ *or Pla2g2d*$^{+/+}$ mice and summary data are shown. Mean ± SEM; two independent experiments with six mice/group. ***, $P < 0.001$ (unpaired Student's *t* test).

middle-aged *Pla2g2d*$^{-/-}$ and *Pla2g2d*$^{+/+}$ mice. A higher frequency and number of virus-specific (epitope S525-specific) CD8 T cell and (epitope N110-specific) CD4 T cells (Fig. 7 A) were present in the lungs of *Pla2g2d*$^{-/-}$ mice compared with *Pla2g2d*$^{+/+}$ mice. In addition, we also observed that CD8 T cells from *Pla2g2d*$^{-/-}$ compared with *Pla2g2d*$^{+/+}$ mice produced more IFN-γ on a per cell basis (Fig. 7 B), although there were no differences in the fraction of CD8 T cells that produced both IFN-γ and TNF (Fig. 7 C). Further, the absence of PLA_2G2D augmented CD8 T cell cytolytic activity, measured in an in vivo killing assay (Fig. 7 D). To investigate if there was also a T cell–intrinsic defect in *Pla2g2d*$^{+/+}$ mice, we performed a set of adoptive transfer experiments, transferring splenocytes from uninfected *Pla2g2d*$^{+/+}$ or *Pla2g2d*$^{-/-}$ mice to CD45 disparate *Pla2g2d*$^{-/-}$ or *Pla2g2d*$^{+/+}$ mice, respectively, before SARS-CoV infection. In each case, the frequency of transferred CD8 T cells that expressed IFN-γ after peptide stimulation was similar to that of endogenous cells, indicating that the defects were T cell extrinsic (Fig. 7 E).

We next assessed whether these enhanced SARS-CoV–specific T cell responses decreased mortality after SARS-CoV infection. To this end, we infected middle-aged *Pla2g2d*$^{-/-}$ and *Pla2g2d*$^{+/+}$ mice with SARS-CoV and monitored survival (Fig. 8 A). More than 80% of *Pla2g2d*$^{-/-}$ mice survived the infection, whereas all *Pla2g2d*$^{+/+}$ mice died. Increased survival reflected enhanced kinetics of viral clearance in *Pla2g2d*$^{-/-}$ mice (Fig. 8 B), mediated by the more robust T cell response observed in these mice. In addition, decreased pathological changes were observed in the lungs of *Pla2g2d*$^{-/-}$ compared with *Pla2g2d*$^{+/+}$ mice. We detected no differences in the lungs of uninfected mice (Fig. 8 C, naive). *Pla2g2d*$^{+/+}$ mice showed much greater perivascular cuffing and cellular infiltration compared with *Pla2g2d*$^{-/-}$ mice by day 4 p.i. By day 6 p.i., multifocal inflammatory lesions around blood vessels and alveolar edema were significantly greater in *Pla2g2d*$^{+/+}$ mice, with few changes observed in *Pla2g2d*$^{-/-}$ mice.

Enhanced rDC migration to MLN and T cell responses in influenza A virus (IAV)–infected *Pla2g2d*$^{-/-}$ mice

To determine whether elevated PLA_2G2D levels in middle-aged mice affected the host immune response to other respiratory pathogens, we infected *Pla2g2d*$^{-/-}$ and *Pla2g2d*$^{+/+}$ mice with IAV (PR8 strain) and monitored rDC migration, T cell responses and survival. Both the frequency and number

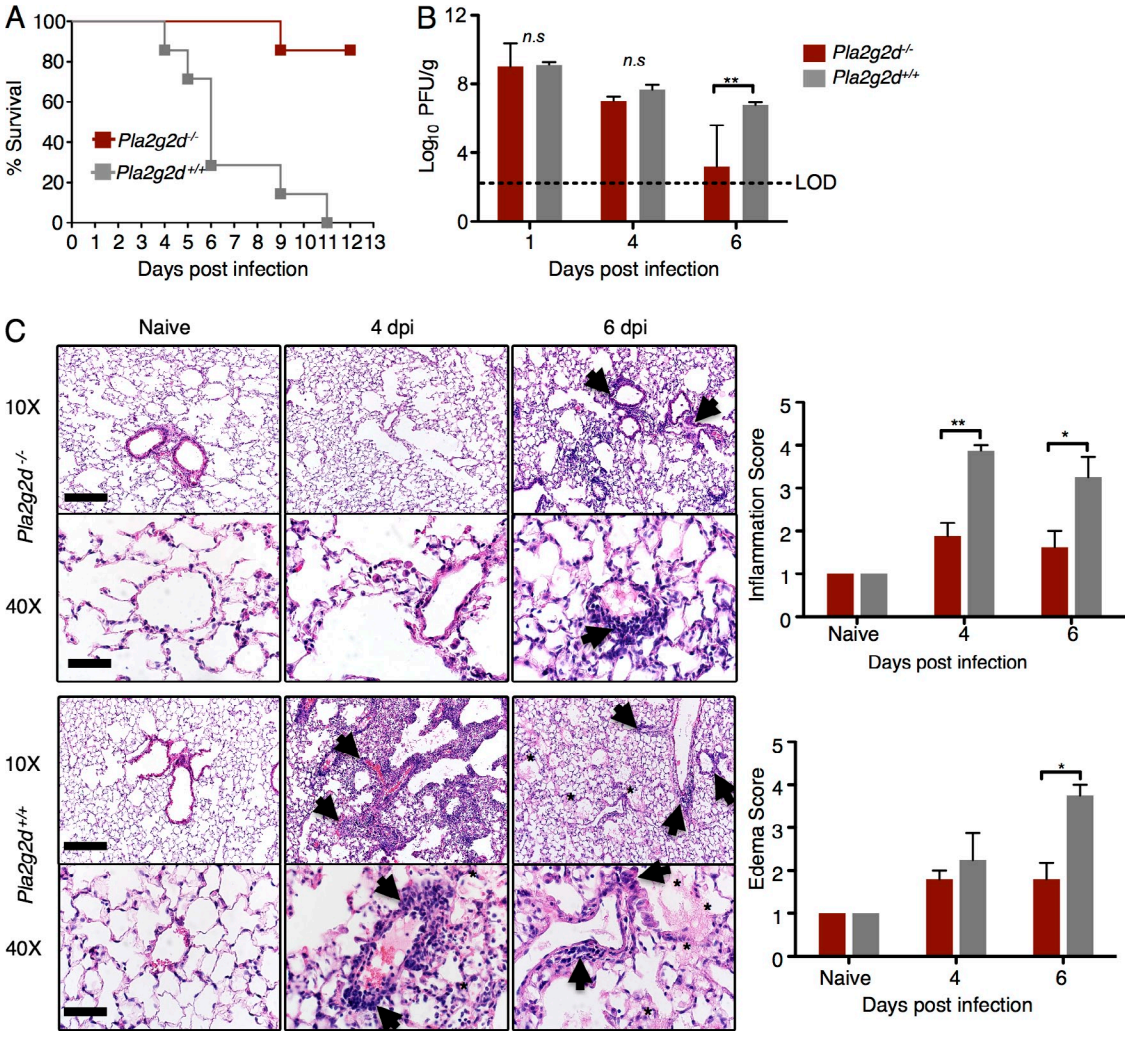

Figure 8. ***Pla2g2d*$^{-/-}$ mice are protected from SARS-CoV infection.** Middle-aged *Pla2g2d*$^{-/-}$ *or Pla2g2d*$^{+/+}$ mice were infected with 10^4 PFU of SARS-CoV i.n. (A) Mice were monitored daily for survival. Data are representative of two independent experiments, seven mice/group. $P < 0.001$ (Kaplan-Meier log-rank survival tests). (B) Viral titers in the lungs of *Pla2g2d*$^{-/-}$ and *Pla2g2d*$^{+/+}$ mice at days 1, 4, and 6 p.i. are shown. Mean ± SEM; two independent experiments, seven mice/group. **, $P < 0.01$ (unpaired Student's *t* test). (C) Lung sections from *Pla2g2d*$^{-/-}$ and *Pla2g2d*$^{+/+}$ mice on day 6 p.i. were analyzed for pathological changes. Infiltrating cells (black arrows) and edema (asterisks) are shown. Histological changes were scored for inflammation and edema as described in Materials and methods. Mean ± SEM; two independent experiments, with three to five mice per group. *, $P < 0.05$; **, $P < 0.01$. Bars: (10×) 300 µm; (40×) 70 µm.

of rDCs were increased in the MLN of *Pla2g2d*$^{-/-}$ compared with *Pla2g2d*$^{+/+}$ mice when assessed at 18 h p.i. (Fig. 9 A). Consistent with increased rDC migration, we found that CD8 T cell responses were significantly higher in the lungs of *Pla2g2d*$^{-/-}$ mice, when measured at 10 d p.i. (Fig. 9 B). Enhancement of the CD8 T cell response did not increase survival in IAV-infected mice (Fig. 9 C). This may occur because the CD8 T cell response is preserved to a greater extent in IAV compared with SARS-CoV–infected middle-aged *Pla2g2d*$^{+/+}$ mice, so that its augmentation has less of an effect on survival (Zhao et al., 2011).

Chronic oxidative stress mediates elevated PLA_2G2D expression

Aging is accompanied by oxidative stress, which triggers lipid peroxidation (Cannizzo et al., 2012). A consequence of lipid peroxidation is increased expression of various PLA_2s (Brown et al., 2003), raising the possibility that increased oxidative stress in the middle-aged lung is a key factor in PLA_2G2D up-regulation. To evaluate whether oxidative stress is increased in the lungs of middle-aged mice, we first measured the levels of malondialdehyde (MDA), a product of lipid peroxidation, and an indicator of oxidative stress (Gutteridge and Halliwell, 1990). Analyses of middle-aged compared with young mice revealed higher lung concentrations of MDA (Imai et al., 2008), indicative of greater pulmonary oxidative stress (Fig. 10 A).

Oxidative stress can be countered by treatment with N-acetyl cysteine (NAC) and, as shown in Fig. 10 B, treatment of middle-aged mice with NAC for 10 d reduced MDA levels. Notably, NAC treatment also diminished levels of PLA_2G2D mRNA in lung CD11c$^+$ cells, suggesting that augmented

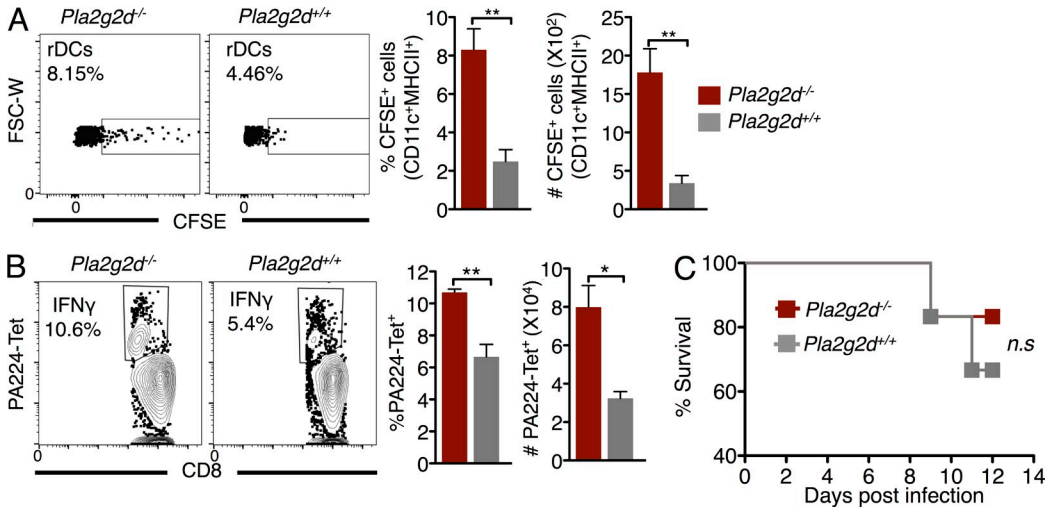

Figure 9. PLA_2G2D dampening of the anti-IAV T cell response. Middle-aged *Pla2g2d*$^{-/-}$ *or Pla2g2d*$^{+/+}$ mice were infected with 1020 tissue culture infectious units of IAV (PR8 strain) and analyzed for differences in rDC migration, CD8 T cell response in lungs, and survival. (A) Flow plots and frequency (left bar graph) and number (right bar graph) of airway DCs ($CD11c^+MHCII^+CFSE^+$) that migrated from the lung to MLN, 18 h after IAV infection. Mean ± SEM; two independent experiments, four mice/group. **, $P < 0.01$, unpaired Student's *t* test. (B) Flow plots and summary data indicate the frequency and numbers of D^b/PA224 tetramer$^+$ CD8 T cells at 10 d p.i. Mean ± SEM; two independent experiments, four mice/group. *, $P < 0.05$; **, $P < 0.01$, unpaired Student's *t* test. (C) Percentage survival. Data are representative of two independent experiments, six mice/group. n.s., not significant (Kaplan-Meier log-rank survival tests).

PLA_2G2D expression in middle-aged mice was related to oxidative stress (Fig. 10 B). Further, to induce oxidative stress in young mice, we treated them for seven days with a low dose of LPS (0.1 µg/mouse; Kratzer et al., 2012). This dose has been shown to result in low level induction of proinflammatory mediators in murine macrophages (Maitra et al., 2012). Chronic LPS treatment resulted in higher concentrations of MDA in the lungs of mice compared with controls (Fig. 10 C). More importantly, inducing oxidative stress with LPS also increased mRNA levels of PLA_2G2D (Fig. 10 C), but not of other PLA2s (PLA_2G4, PLA_2G2E, PLA_2G10; Fig. 10 D) in lung $CD11c^+$ cells.

To extend the clinical relevance of these results, we next determined whether chronic oxidative stress resulted in PLA_2G2D up-regulation in human monocyte-derived macrophages (MDMs). For this purpose, PBMCs were treated with macrophage colony stimulating factor (M-CSF) for 4 d, and the cell-adherent population was incubated with M-CSF in the presence or absence of low levels of LPS (0.1 ng/ml) for an additional 1–10 d. PLA_2G2D expression was then assessed. In agreement with previous work (Miki et al., 2013), LPS exposure for 1 d did not result in increased PLA_2G2D levels (unpublished data). However, we observed increased PLA_2G2D expression after chronic LPS treatment (10 d), and this was accompanied by increases in MDA levels, indicative of higher oxidative stress (Fig. 10 E). Thus, chronic oxidative stress, a well-described aspect of aging in the human lung, results in increased PLA_2G2D levels, which could contribute to age-dependent defects in the immune response to SARS-CoV and other respiratory pathogens.

DISCUSSION

Although many infections are more severe in aged populations, SARS, and possibly MERS show remarkable age-dependent differences in outcomes such that young humans (less than 24 yr) all survived the infection, whereas 15% and 52% of middle-aged and aged individuals, respectively, succumbed (Peiris et al., 2004; Assiri et al., 2013; Saad et al., 2014; Alsolamy, 2015). SARS-CoV–infected mice also show similar steep age-dependent changes in mortality, which we show is due, in large part, to increases in levels of a single secretory PLA_2, PLA_2G2D, as mice age. A hallmark of aging is lipid peroxidation and subsequent up-regulation of PLA_2s (Brown et al., 2003; Sun et al., 2004; Hermann et al., 2014) and our results suggest that, in the lungs, levels of PLA_2G2D singularly increase as mice age. PLA_2G2D is considered an antiinflammatory/proresolving enzyme, suggesting its up-regulation is actually a measure used in the lung to counter the low-grade chronic inflammation that occurs with aging (Franceschi et al., 2000; Miki et al., 2013). In support of this notion, treatment with low doses of LPS, which induces oxidative stress and low-grade inflammation, resulted in PLA_2G2D up-regulation both in $CD11c^+$ cells in the mouse lung (Fig. 10 C) and in human monocyte-derived macrophages (Fig. 10 E). Further, interventions that diminish reactive oxygen species decreased PLA_2G2D expression (Fig. 10 B). A recent study demonstrated the proresolving role of PLA_2G2D in the setting of contact dermatitis in mice; in its absence, resolution was prolonged (Miki et al., 2013). PLA_2G2D would be expected to have similar effects in ameliorating disease in the context of autoimmune disease.

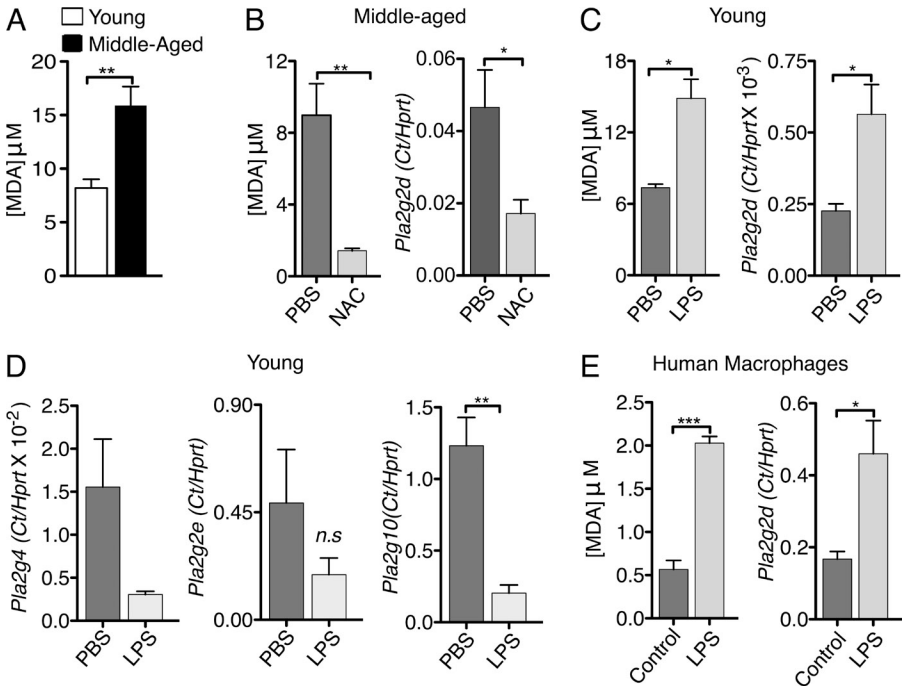

Figure 10. Oxidative stress induces expression of PLA_2G2D. A TBARS assay was used to measure lung MDA concentrations as a measure of oxidative stress in mouse lungs and human MDMs. (A) MDA concentration in the lungs of naive young and middle-aged mice. Mean ± SEM; two independent experiments, four mice/group. **, P < 0.01, unpaired Student's *t* test. (B) $CD11c^+$ cells from the lungs of naive middle-aged mice that were treated with NAC or PBS (control) i.n. for 10 d, were separated using magnetic beads and expression of PLA_2G2D was determined by qPCR and lung MDA concentrations were measured by TBARS assay. Mean ± SEM; two independent experiments, four mice/group. *, P < 0.05; **, P < 0.01 (unpaired Student's *t* test). (C and D) $CD11c^+$ cells from the lungs of naive young mice that were treated with low doses of LPS or PBS (control) i.n. for 7 d were separated using magnetic beads. Expression of PLA_2G2D (C) and other PLA2s (D) was determined by qPCR and lung MDA concentrations were measured by TBARS assay. Mean ± SEM; two independent experiments, six mice/group. n.s., not significant; *, P < 0.05; **, P < 0.01 (unpaired Student's *t* test). (E) Human MDMs were treated with low doses of LPS and MDA concentration (left) and *Pla2g2d* expression (right) were measured as before. Mean ± SEM; two independent experiments, three human PBMC samples with four replicates/sample. *, P < 0.05; ***, P < 0.001, unpaired Student's *t* test.

Increased PLA_2G2D expression by lung $CD11c^+$ cells results in up-regulation of several eicosanoids, with especially prominent effects on PGD_2 production (Figs. 4 D and 5, E and H). Activation of the PGD_2–DP1 signaling axis on rDCs results in decreased CCR7 expression so that DP1 antagonism results in augmented rDC migration to the draining LN in uninfected and SARS-CoV–infected mice (Hammad et al., 2003; Zhao et al., 2011). Of note, inhibition of DC migration by PGD_2/DP1 signaling is not confined to the lung, because, after skin invasion, *Schistoma mansonii* releases PGD_2 to inhibit Langerhans cell migration to the draining LN, delaying the initial immune response (Angeli et al., 2001). Similar effects are observed in $Pla2g2d^{-/-}$ mice infected with either SARS-CoV or IAV, resulting in enhanced T cell responses (Fig. 7, A, B, and D, and 9 B) and, in the case of SARS-CoV, improved survival (Fig. 8 A). In addition, PGD_2 can also mediate its antiinflammatory effects through binding of 15d-PGJ_2, a dehydration end product of PGD_2, to a nuclear receptor PPARγ (Hilliard et al., 2010).

Although we primarily focused on the role of PLA_2G2D in increased PGD_2 production, PLA_2G2D is critical for the synthesis of additional antiinflammatory/proresolving molecules. PUFA–oxygenated metabolites with dedicated proresolving activities, including resolvins, protectins, and maresins (also called specialized proresolving mediators [SPMs]), are derived from ω3 fatty acids such as EPA and DHA (Serhan et al., 2002; Buckley et al., 2014; Serhan, 2014). PLA_2G2D is known to release free PUFAs into a substrate pool that can be further mobilized to produce proresolving lipid mediators such as DHA-derived resolvin D1 and EPA-derived resolvin E1 among many others (Serhan et al., 2002; Miki et al., 2013). Notably, EPA levels were higher in the lungs of uninfected middle-aged compared with young mice (Fig. 4 B), and both EPA and DHA production were higher in uninfected and infected $Pla2g2d^{+/+}$ mice compared with their $Pla2g_2d^{-/-}$ counterparts (Figs. 4 H and 5 F). However we failed to detect any resolvins or protectins, the downstream metabolites of EPA or DHA in the lungs of mice, possibly reflecting low levels of these molecules in lung tissue. Notably, although EPA is higher in middle-aged compared with young lungs (DHA is nearing to significance; P = 0.12; Fig. 4 B), SPMs are lower in the uninflamed peritoneum of aged compared with young mice (Arnardottir et al., 2014), suggesting that age-dependent differences in baseline levels of these molecules are organ-specific and could possibly contribute to disease-specific outcomes.

Our results also indicated that age-dependent differences in lung PLA_2G2D levels were confined to $CD11c^+$ cells. $CD11c^+$ cells in draining LN also express PLA_2G2D, and relative levels are much higher than in the lung (Miki et al., 2013), but these do not change as mice age (Fig. 2 F). This specific

effect of aging on pulmonary CD11c$^+$ cells may reflect constant exposure to airborne antigens, most of which are innocuous. An immune response to these antigens would be undesirable and would contribute to allergic reactions and asthma. In contrast, PLA_2G2D in lymph nodes might be expected to have a different role, namely to down-regulate proinflammatory responses, and thereby contribute to resolution of the immune response after pathogen control or allergic or autoimmune reactions.

A key question is why SARS-CoV–infected mice are especially affected by age-dependent changes in PLA_2G2D expression. One unique feature of SARS is that maximal virus titers in mouse lungs are detected within 24 h after infection (Fett et al., 2013), nearly coincident with the time of maximal migration of rDCs from the lungs to the DLNs. Furthermore, coronavirus replication results in extensive membrane remodeling with the formation of double membrane vesicles and other membranous structures, the sites of viral RNA synthesis and assembly (Novoa et al., 2005; Knoops et al., 2008; Miller and Krijnse-Locker, 2008). This virus-induced reorganization of the host cell membrane causes the accumulation of cone-shaped lipids, specifically lysophosphatidylcholine (LPC) or phosphatidylethanolamine (PE; Escribá et al., 1997; Lee and Ahlquist, 2003; Diaz et al., 2010; Lorizate and Kräusslich, 2011; Xu and Nagy, 2015). Because PLA_2G2D specifically mobilizes PE to release AA and DHA (Miki et al., 2013), robust replication of SARS-CoV during the first 24 h of infection likely increases the amount of PLA_2G2D substrate. Additionally, LPC and PE may form large lipid aggregates; most secreted phospholipases, including PLA_2G2D, exhibit a tendency to show increased activity when the substrate is presented in this form (Carman et al., 1995; Gelb et al., 1995). Thus, SARS-CoV infection results in enhanced release of AA into the eicosanoid pathway, which increases the concentration of PGD_2 and downstream products of EPA and DHA, further dampening the immune response. Notably, similar processes may occur in patients with MERS-CoV infections, who also exhibit age-dependent increases in susceptibility (Assiri et al., 2013; Saad et al., 2014; Alsolamy, 2015).

In conclusion, it is likely that in the absence of challenge with a pathogen such as SARS-CoV, elevated PLA_2G2D expression benefits the host by increasing the level of various immunosuppressive lipid mediators such as PGD_2, thereby dampening the response to environmental antigens. However in the context of an infection, the higher basal levels of PGD_2 and other proresolving lipid mediators adversely affect the initiation of a protective innate immune response and ultimately adaptive immune response (Fig. 10 E). Thus, therapeutic interventions that increase the levels of proresolving lipid mediators might have undesirable effects in the context of infection. However, these results also suggest that PLA_2G2D would serve as a useful therapeutic target in the lungs of patients after infection with SARS-CoV and perhaps other respiratory viral pathogens, including MERS-CoV. Short-term targeting of a single inducible PLA_2 would avoid undesirable effects that might be observed by generalized inhibition of PLA_2 function. Such drugs have been developed for some PLA_2s (Oslund et al., 2008), although not yet for PLA_2G2D, demonstrating the feasibility of this approach.

MATERIALS AND METHODS

Mice, virus, and infection. 6 wk to 22 mo specific pathogen–free C57BL/6 mice were purchased from Charles River Laboratories or the National Cancer Institute (National Institutes of Health). *Pla2g2d*$^{-/-}$ and *Pla2g2d*$^{+/+}$ mice (H-2^b) were generated as described (Miki et al., 2013). After initial development, mice were backcrossed greater than 12 times to C57BL/6NCrSLc mice. *Pla2g2d*$^{+/+}$ C57BL/6NCrSLc mice were used as controls for all experiments. Mouse-adapted SARS-CoV (MA15) and IAV A/PR8/34 were obtained from Kanta Subbarao (National Institutes of Health) and Kevin Legge (University of Iowa, Iowa City, IA), respectively. For infections, mice were lightly anesthetized using isoflurane and infected i.n. with 1×10^4 PFU SARS-CoV or 10^3 TCID IAV in a 50 µl volume. All animal studies were approved by the University of Iowa Animal Care and Use Committee and meet stipulations of the Guide for the Care and Use of Laboratory Animals.

Virus titration. Lungs were harvested on the indicated days p.i. Tissue was homogenized in PBS using a manual homogenizer and titered on Vero E6 cells. For plaque assays, cells were fixed with 10% formaldehyde and stained with crystal violet 3 d p.i. Viral titers are expressed as PFU/gram.

CD11c$^+$ cell magnetic bead separation. Lung single-cell suspensions were prepared as described. CD11c$^+$ cells were separated using anti–mouse CD11c MicroBeads (Miltenyi Biotec) following the manufacturer's protocol.

Microarray analysis. CD11c$^+$ cells from the lungs of young and middle-aged mice were separated as described above. RNA was purified using a mirVana kit (Life Technologies) according to the manufacturer's instructions. RNA samples were assessed for purity and quality using an Agilent 2100 Bioanalyzer. RNA for the microarray was processed using a NuGEN WT-Ovation Pico RNA Amplification System together with a NuGEN WT-Ovation Exon Module. Samples were hybridized and loaded onto MouseRef-8 v2.0 Expression BeadChip (Illumina). Arrays were scanned with a HiScan bead array system, and data were collected using GeneChip Operating Software.

Data from Illumina MouseRef-8 v2.0 Expression BeadChip were normalized and median polished using Robust Multichip Average background correction with $\log_2$-adjusted values. After obtaining the $\log_2$ expression values for genes, significance testing was performed comparing the two groups (CD11c$^+$ cells from lungs of young and middle-aged mice). False discovery rate was applied to all p-values to correct for multiple testing. Significance of expression differences was assessed using an false discovery rate (FDR) cutoff of 0.05 and a twofold change. Analysis and visualization of data and pathway analysis were performed using PartekGS software and Ingenuity Pathway Analysis software. Complete microarray data have been deposited at the Gene Expression Omnibus under accession no. GSE71868.

In situ CFSE and OVA-FITC staining. CFSE and OVA-FITC were purchased from Molecular Probes. CFSE was diluted to a concentration of 8 mM in DMEM, and then administered i.n. (50 µl) 6 h before infection (Legge and Braciale, 2005; Zhao et al., 2011). OVA-FITC was dissolved in PBS, and 200 µg were administered i.n. in 75 µl.

Lung and lymph node preparation. Mice were euthanized at the indicated time points. After perfusion through the right ventricle with 5 ml of PBS, lungs and DLNs were removed. Lungs were diced into small pieces and digested in HBSS buffer containing 2% FCS, 25 mM HEPES, 1 mg/ml Collagenase D (Roche) and 0.1 mg/ml DNase (Roche) for 30 min at 37°C. After pressing through 70 µm nylon filters, lungs homogenates were spun down and treated with red blood cell lysis buffer. Cells were counted using a hemocytometer after dilution in 0.2% Trypan blue. Lymph nodes were dispersed and single-cell suspensions prepared using 70 µm nylon filters and counted.

Lung histology. Animals were anesthetized and transcardially perfused with PBS followed by zinc formalin. Lungs were removed, fixed in zinc formalin, and paraffin embedded. Sections were stained with hematoxylin and eosin and examined by light microscopy. Images were acquired using a BX53 microscope (Olympus), DP73 camera (Olympus), and CellSens software (Olympus). All sections were examined at room temperature using 10× or 40× objective lens. Sections were evaluated by a veterinary lung pathologist using postexamination masking techniques (Gibson-Corley et al., 2013). Sections were scored as follows: Inflammation, 1, normal range; 2, focal small patches of perivascular leukocyte aggregates (0–33% of lung); 3, multifocal patches of perivascular leukocyte aggregates (33–66% of lung); 4, widespread patches of perivascular leukocyte aggregates (>67% of lung). Edema: 1, none; 2, minor (0–33% lung fields); 3, (33–66% lung fields); 4, (>67% lung fields).

Antibodies and flow cytometry. The following monoclonal antibodies were used: PE or PercP Cy5.5-conjugated rat anti–mouse CD4 (RM4-5), FITC-conjugated rat anti–mouse CD8 (53–6.7), FITC or e450-conjugated hamster anti–mouse CD11c (HL3), APC or e450-conjugated rat anti–mouse CD11b, and rat anti–mouse CD16/32 (2.4G2) (eBioScience); PercP Cy5.5-conjugated hamster anti–mouse CD3 (145-2C11), PercP Cy5.5-conjugated rat anti–mouse I-A/I-E (M5/114.15.2), PercP Cy5.5 or PE-conjugated rat anti–mouseCD45 (30-F11), Alexa Fluor 647 or APC-conjugated rat anti–mouse IFN-γ (XMG1.2), and APC-conjugated rat anti–mouse TNF (MP6-XT22; BioLegend); PE or FITC-conjugated hamster anti–mouse CD80 (16-10A1), and FITC-conjugated rat anti–mouse CD40 (1C 10; BD). For PLA_2G2D staining, rabbit anti–mouse PLA_2G2D antibody (Miki et al., 2013) was used as primary antibody, followed by staining with Alexa Fluor 647-conjugated goat anti–rabbit (Life Technologies).

For surface staining, 1×10^6 cells were blocked with 1 µg of anti-CD16/32 antibody and stained with the indicated antibodies at 4°C, except for anti-CCR7 antibody, which was used at 37°C. After washing, cells were fixed using Cytofix Solution (BD). To detect antigen-specific T cells after SARS-CoV infection, 1×10^6 cells were cultured in a 96-well round bottom plate in the presence of Brefeldin A and peptides corresponding to a CD8 T cell epitope (S525) or a CD4 T cell epitope (N110; Bio-Synthesis). To assess the functionality of $CD11c^+$ cells, lung cells were prepared as described above and stimulated with LPS (1 µM), poly I:C (10 µg/ml), or vehicle (RP10) in the presence of Brefeldin A for 6 h at 37°C. To determine the frequency of $CD11c^+$ cells expressing PLA_2G2D, lung cells were incubated for 6 h at 37°C in the presence of Brefeldin A. Cells were then fixed and permeabilized using Cytofix/Cytoperm (BD) and labeled with anti–IFN-γ (T cells), anti-TNF ($CD11c^+$ cells) or anti-PLA_2G_2D antibody. To detect antigen-specific T cells after IAV infection, lung cells were prepared as described above and PA224-specific CD8 T cells were identified by staining with $H2D^b$/PA224 tetramer (National Institute of Allergy and Infectious Diseases Tetramer Facility, Atlanta, GA). Flow cytometric data were acquired using a FACSVerse (BD) and were analyzed using FlowJo software (Tree Star).

PCR and primers. Total RNA was extracted from $CD11c^+$ and $CD11c^-$ lung cells or whole lungs of naive or SARS-CoV–infected mice at the specified time p.i. using TRIzol reagent (Invitrogen). 2 µg of RNA were used for cDNA synthesis. 2 µl of cDNA were added to 23 µl of PCR cocktail containing 2XSYBR Green Master Mix (ABI) and 0.2 µM of forward and reverse primer. Amplification was performed in an ABI Prism 7700 thermocycler. The list of genes and of forward and reverse primers is shown in Table S2. Cycle threshold (Franceschi et al., 2000) values were normalized to those of the housekeeping gene hypoxanthine phosphoribosyltransferase (HPRT) by the following equation: $\Delta Ct = Ct_{(\text{gene of interest})} - Ct_{(\text{HPRT})}$. All results are shown as a ratio to HPRT calculated as $2^{-(\Delta Ct)}$.

LC/MS. Lungs were harvested into 2 ml methanol and homogenized using a tissue grinder. 200 µl were transferred to a second tube and diluted to a final volume of 3 ml of 60% methanol (vol/vol). After incubation for 30 min at 37°C, 100 µl (0.1 ng/µl) of internal standard cocktail was added. Samples were diluted to a final concentration of 10% methanol (vol/vol) with water. For AA, PGD_2, PGE_2, PGF2α, TXB_2, and 6-keto-PGF1α, internal standards were AA-d8, PGD_2-d4, PGE_2-d4, PGF2α-d4, TXB_2-d4, and 6-keto-PGF1α-d4, respectively, all purchased from Cayman Chemical and added at the aforementioned concentration. For DHA and EPA, LTB_4-d4 was used as the internal standard. Samples were centrifuged at 3,000 rpm for 10 min and the supernatant was subjected to solid phase extraction using a Strata-X 33 µm Polymeric Reversed Phase columns (60 mg/3 ml). Columns were purchased from Phenomenex, activated with 3 ml methanol, and washed with 3 ml water. Samples were eluted with 1 ml methanol, vacuum dried, and resuspended in 100 µl of mobile phase A. The analyses of PUFAs and their metabolites were performed using a Waters Acquity triple quadrupole mass spectrometer coupled with liquid chromatography (Acquity H class UPLC). Samples were then applied to an Acquity UPLC BEH C18 column (130 Å, 1.7 µm, 2.1 mm × 100 mm) and fractionated using a step gradient with mobile phase A (63:37:0.02% water/acetonitrile/formic acid) and mobile phase B (1:1 acetonitrile/isopropanol) at a flow rate of 300 µl/min for most analytes. For DHA and EPA, the mobile phase A was 65:35:0.01% methanol/water/acetic acid and mobile phase B was 100% methanol with 0.01% acetic acid. Columns were run at a flow rate of 250 µl/min. Primary standards were analyzed in parallel with the samples to enable quantification of the endogenous lipids. Detection of each lipid was performed by multiple reaction monitoring.

Adoptive transfer of bulk splenocytes. Naive CD45.1 (*Pla2g2d*$^{+/+}$) or CD45.2 (*Pla2g2d*$^{-/-}$) splenocytes were adoptively transferred by intravenous inoculation into CD45.2 (*Pla2g2d*$^{-/-}$) or CD45.1 (*Pla2g2d*$^{+/+}$) mice, respectively, at 50×10^6 cells/mouse. 1 d after transfer, mice were infected with SARS-CoV i.n. Lungs were harvested 6 dpi and analyzed for virus-specific T cells as described in the preceding sections.

In vivo cytotoxicity assay. This assay was performed as described previously (Barber et al., 2003). In brief, splenocytes from CD45.1 mice (*Pla2g2d*$^{+/+}$, WT) were stained with high (1 µM, $CFSE^{hi}$) or low (100 nM, $CFSE^{lo}$) concentrations of CFSE. $CFSE^{hi}$ cells were then pulsed with S525 (10 µM) at 37°C for 1 h. 5×10^5 cells from each group ($CFSE^{hi}$ and $CFSE^{lo}$) were mixed together (10^6 cells total) and transferred i.n. into mice CD45.2 *Pla2g2d*$^{+/+}$ and *Pla2g2d*$^{-/-}$ mice at 6 d p.i. Lungs were harvested 12 h later and analyzed for numbers of $CFSE^{hi}$ and $CFSE^{lo}$ CD45.1 cells. Percentage killing was calculated using the formula: 100 − ([% peptide pulsed in infected/% unpulsed in infected]/[% peptide pulsed in uninfected/% unpulsed in uninfected]) × 100) (Barber et al., 2003).

LPS treatment. Young mice (6–8 wk) were treated i.n. with LPS (*E. coli* O111:B4) at 0.1 µg/mouse in 50 µl for 7 d.

Antioxidant treatment. Middle-aged mice (10–13 mo) were treated with *N*-Acetyl-L-Cysteine (Sigma-Aldrich; 100 mg/kg, i.p.) for 7 d.

TBARS assay. Pulmonary oxidative stress was measured using a TBARS assay kit according to the manufacturer's protocol (Cayman Chemicals). Data are expressed as the concentration of MDA (Imai et al., 2008) in infected lungs.

Human monocyte-derived macrophages. Human peripheral blood samples from leukocyte reduction cones were obtained from anonymous volunteers that had consented to blood donation at the DeGowin Blood Center at the University of Iowa. Consent forms were approved by the University of Iowa's Institutional Review Board. To obtain monocytes, PBMCs were cultured in tissue culture plates at a seeding density of 1×10^6 cells/ml in RP-10 media (RPMI-1640 medium [Invitrogen] with 10% FBS [Atlanta Biologicals] and 2 mM L-glutamine) supplemented with 5 ng/ml M-CSF (eBioscience) at 37°C with 5% CO_2. After 4 d, the plates were washed with Hanks's balanced salt solution devoid of divalent cations (Invitrogen) to remove nonadherent cells. Adherent cells (predominantly MDMs)

were then trypsinized and pelleted. Pelleted MDMs were resuspended at 1 × 10^6 cells/ml in RP10 supplemented with M-CSF (5 ng/ml) and incubated at 37°C overnight. MDMs were subsequently seeded at a density of 5 × 10^5/ml and incubated for 10 h at 37°C and 5% CO_2. MDMs were then treated with 0.1 nM LPS (*E. coli* O111:B4; Sigma-Aldrich) and M-CSF (1 ng/ml) daily for 10 d.

Statistics. A Student's *t* test was used to analyze differences in mean values between groups except in the case of the microarray data. All results are expressed as mean ± SEM. P-values of <0.05 were considered statistically significant. *, $P < 0.05$; **, $P < 0.01$; ***, $P < 0.001$. Differences in mortality were analyzed using Kaplan-Meier log-rank survival tests. Microarray data were subjected to multiple comparisons and FDR is shown, as described above.

Online supplemental material. Fig. S1 is a schematic representation of the effects of PLA_2G2D in lungs of mice during SARS-CoV infection. Table S1 shows a list of genes in pulmonary $CD11c^+$ cells expressed differentially in young and middle-aged mice. Table S2 shows qPCR primer sequences used in this study. Online supplemental material is available at http://www.jem.org/cgi/content/full/jem.20150632/DC1.

We thank Drs. Anthony Fehr, Rudragouda Channappanavar, Jincun Zhao and Kevin Legge for critical review of the manuscript and Dr. Ramakrishna Sompallae for help with the statistical analyses.

This work was supported by grants from the National Institutes of Health (AI060699, AI091322, S. Perlman; HL36235, M. Gelb) and by grants-in aid for Scientific Research from the Ministry of Education, Culture, Sports, Science and Technology of Japan (22116005, 24390021) and Core Research for Evolutional Science and Technology from the Japan Science and Technology Agency.

The authors declare no competing financial interests.

Submitted: 7 April 2015
Accepted: 19 August 2015

REFERENCES

Alsolamy, S. 2015. Middle East respiratory syndrome: knowledge to date. *Crit. Care Med.* 43:1283–1290. http://dx.doi.org/10.1097/CCM.0000000000000966

Angeli, V., C. Faveeuw, O. Roye, J. Fontaine, E. Teissier, A. Capron, I. Wolowczuk, M. Capron, and F. Trottein. 2001. Role of the parasite-derived prostaglandin D2 in the inhibition of epidermal Langerhans cell migration during schistosomiasis infection. *J. Exp. Med.* 193:1135–1147. http://dx.doi.org/10.1084/jem.193.10.1135

Arita, M., M. Yoshida, S. Hong, E. Tjonahen, J.N. Glickman, N.A. Petasis, R.S. Blumberg, and C.N. Serhan. 2005. Resolvin E1, an endogenous lipid mediator derived from omega-3 eicosapentaenoic acid, protects against 2,4,6-trinitrobenzene sulfonic acid-induced colitis. *Proc. Natl. Acad. Sci. USA.* 102:7671–7676. http://dx.doi.org/10.1073/pnas.0409271102

Arnardottir, H.H., J. Dalli, R.A. Colas, M. Shinohara, and C.N. Serhan. 2014. Aging delays resolution of acute inflammation in mice: reprogramming the host response with novel nano-proresolving medicines. *J. Immunol.* 193:4235–4244. http://dx.doi.org/10.4049/jimmunol.1401313

Assiri, A., J.A. Al-Tawfiq, A.A. Al-Rabeeah, F.A. Al-Rabiah, S. Al-Hajjar, A. Al-Barrak, H. Flemban, W.N. Al-Nassir, H.H. Balkhy, R.F. Al-Hakeem, et al. 2013. Epidemiological, demographic, and clinical characteristics of 47 cases of Middle East respiratory syndrome coronavirus disease from Saudi Arabia: a descriptive study. *Lancet Infect. Dis.* 13:752–761.

Barber, D.L., E.J. Wherry, and R. Ahmed. 2003. Cutting edge: rapid in vivo killing by memory CD8 T cells. *J. Immunol.* 171:27–31. http://dx.doi.org/10.4049/jimmunol.171.1.27

Brown, W.J., K. Chambers, and A. Doody. 2003. Phospholipase A2 (PLA2) enzymes in membrane trafficking: mediators of membrane shape and function. *Traffic.* 4:214–221. http://dx.doi.org/10.1034/j.1600-0854.2003.00078.x

Buckley, C.D., D.W. Gilroy, and C.N. Serhan. 2014. Proresolving lipid mediators and mechanisms in the resolution of acute inflammation. *Immunity.* 40:315–327. http://dx.doi.org/10.1016/j.immuni.2014.02.009

Cannizzo, E.S., C.C. Clement, R. Sahu, C. Follo, and L. Santambrogio. 2011. Oxidative stress, inflamm-aging and immunosenescence. *J. Proteomics.* 74:2313–2323. http://dx.doi.org/10.1016/j.jprot.2011.06.005

Cannizzo, E.S., C.C. Clement, K. Morozova, R. Valdor, S. Kaushik, L.N. Almeida, C. Follo, R. Sahu, A.M. Cuervo, F. Macian, and L. Santambrogio. 2012. Age-related oxidative stress compromises endosomal proteostasis. *Cell Reports.* 2:136–149. http://dx.doi.org/10.1016/j.celrep.2012.06.005

Carman, G.M., R.A. Deems, and E.A. Dennis. 1995. Lipid signaling enzymes and surface dilution kinetics. *J. Biol. Chem.* 270:18711–18714. http://dx.doi.org/10.1074/jbc.270.32.18711

Caruso, C., S. Buffa, G. Candore, G. Colonna-Romano, D. Dunn-Walters, D. Kipling, and G. Pawelec. 2009. Mechanisms of immunosenescence. *Immun. Ageing.* 6:10. http://dx.doi.org/10.1186/1742-4933-6-10

Channappanavar, R., J. Zhao, and S. Perlman. 2014. T cell-mediated immune response to respiratory coronaviruses. *Immunol. Res.* 59:118–128. http://dx.doi.org/10.1007/s12026-014-8534-z

Chen, J., and K. Subbarao. 2007. The Immunobiology of SARS. *Annu. Rev. Immunol.* 25:443–472. http://dx.doi.org/10.1146/annurev.immunol.25.022106.141706

Day, C.W., R. Baric, S.X. Cai, M. Frieman, Y. Kumaki, J.D. Morrey, D.F. Smee, and D.L. Barnard. 2009. A new mouse-adapted strain of SARS-CoV as a lethal model for evaluating antiviral agents in vitro and in vivo. *Virology.* 395:210–222. http://dx.doi.org/10.1016/j.virol.2009.09.023

De la Fuente, M., and J. Miquel. 2009. An update of the oxidation-inflammation theory of aging: the involvement of the immune system in oxi-inflamm-aging. *Curr. Pharm. Des.* 15:3003–3026. http://dx.doi.org/10.2174/138161209789058110

Diaz, A., X. Wang, and P. Ahlquist. 2010. Membrane-shaping host reticulon proteins play crucial roles in viral RNA replication compartment formation and function. *Proc. Natl. Acad. Sci. USA.* 107:16291–16296. http://dx.doi.org/10.1073/pnas.1011105107

Donnelly, C.A., A.C. Ghani, G.M. Leung, A.J. Hedley, C. Fraser, S. Riley, L.J. Abu-Raddad, L.M. Ho, T.Q. Thach, P. Chau, et al. 2003. Epidemiological determinants of spread of causal agent of severe acute respiratory syndrome in Hong Kong. *Lancet.* 361:1761–1766. http://dx.doi.org/10.1016/S0140-6736(03)13410-1

Escribá, P.V., A. Ozaita, C. Ribas, A. Miralles, E. Fodor, T. Farkas, and J.A. García-Sevilla. 1997. Role of lipid polymorphism in G protein-membrane interactions: nonlamellar-prone phospholipids and peripheral protein binding to membranes. *Proc. Natl. Acad. Sci. USA.* 94:11375–11380. http://dx.doi.org/10.1073/pnas.94.21.11375

Fainaru, O., D. Shseyov, S. Hantisteanu, and Y. Groner. 2005. Accelerated chemokine receptor 7-mediated dendritic cell migration in Runx3 knockout mice and the spontaneous development of asthma-like disease. *Proc. Natl. Acad. Sci. USA.* 102:10598–10603. http://dx.doi.org/10.1073/pnas.0504787102

Fett, C., M.L. DeDiego, J.A. Regla-Nava, L. Enjuanes, and S. Perlman. 2013. Complete protection against severe acute respiratory syndrome coronavirus-mediated lethal respiratory disease in aged mice by immunization with a mouse-adapted virus lacking E protein. *J. Virol.* 87:6551–6559. http://dx.doi.org/10.1128/JVI.00087-13

Franceschi, C., M. Bonafè, S. Valensin, F. Olivieri, M. De Luca, E. Ottaviani, and G. De Benedictis. 2000. Inflamm-aging. An evolutionary perspective on immunosenescence. *Ann. N. Y. Acad. Sci.* 908:244–254. http://dx.doi.org/10.1111/j.1749-6632.2000.tb06651.x

Frieman, M.B., J. Chen, T.E. Morrison, A. Whitmore, W. Funkhouser, J.M. Ward, E.W. Lamirande, A. Roberts, M. Heise, K. Subbarao, and R.S. Baric. 2010. SARS-CoV pathogenesis is regulated by a STAT1 dependent but a type I, II and III interferon receptor independent mechanism. *PLoS Pathog.* 6:e1000849. http://dx.doi.org/10.1371/journal.ppat.1000849

Frieman, M., B. Yount, S. Agnihothram, C. Page, E. Donaldson, A. Roberts, L. Vogel, B. Woodruff, D. Scorpio, K. Subbarao, and R.S. Baric. 2012. Molecular determinants of severe acute respiratory syndrome coronavirus pathogenesis and virulence in young and aged mouse models of human disease. *J. Virol.* 86:884–897. http://dx.doi.org/10.1128/JVI.05957-11

Gelb, M.H., M.K. Jain, A.M. Hanel, and O.G. Berg. 1995. Interfacial enzymology of glycerolipid hydrolases: lessons from secreted phospholipases A2. *Annu. Rev. Biochem.* 64:653–688. http://dx.doi.org/10.1146/annurev.bi.64.070195.003253

Gibson-Corley, K.N., A.K. Olivier, and D.K. Meyerholz. 2013. Principles for valid histopathologic scoring in research. *Vet. Pathol.* 50:1007–1015. http://dx.doi.org/10.1177/0300985813485099

Gosset, P., M. Pichavant, C. Faveeuw, F. Bureau, A.-B. Tonnel, and F. Trottein. 2005. Prostaglandin D2 affects the differentiation and functions of human dendritic cells: impact on the T cell response. *Eur. J. Immunol.* 35:1491–1500. http://dx.doi.org/10.1002/eji.200425319

Gutteridge, J.M., and B. Halliwell. 1990. The measurement and mechanism of lipid peroxidation in biological systems. *Trends Biochem. Sci.* 15:129–135. http://dx.doi.org/10.1016/0968-0004(90)90206-Q

Hamilton-Easton, A., and M. Eichelberger. 1995. Virus-specific antigen presentation by different subsets of cells from lung and mediastinal lymph node tissues of influenza virus-infected mice. *J. Virol.* 69: 6359–6366.

Hammad, H., H.J. de Heer, T. Soullie, H.C. Hoogsteden, F. Trottein, and B.N. Lambrecht. 2003. Prostaglandin D2 inhibits airway dendritic cell migration and function in steady state conditions by selective activation of the D prostanoid receptor 1. *J. Immunol.* 171:3936–3940. http://dx.doi.org/10.4049/jimmunol.171.8.3936

Hammad, H., M. Kool, T. Soullié, S. Narumiya, F. Trottein, H.C. Hoogsteden, and B.N. Lambrecht. 2007. Activation of the D prostanoid 1 receptor suppresses asthma by modulation of lung dendritic cell function and induction of regulatory T cells. *J. Exp. Med.* 204:357–367. http://dx.doi.org/10.1084/jem.20061196

Hermann, P.M., S.N. Watson, and W.C. Wildering. 2014. Phospholipase A2 - nexus of aging, oxidative stress, neuronal excitability, and functional decline of the aging nervous system? Insights from a snail model system of neuronal aging and age-associated memory impairment. *Front. Genet.* 5:419. http://dx.doi.org/10.3389/fgene.2014.00419

Hilliard, M., C. Frohnert, C. Spillner, S. Marcone, A. Nath, T. Lampe, D.J. Fitzgerald, and R.H. Kehlenbach. 2010. The anti-inflammatory prostaglandin 15-deoxy-delta(12,14)-PGJ2 inhibits CRM1-dependent nuclear protein export. *J. Biol. Chem.* 285:22202–22210. http://dx.doi.org/10.1074/jbc.M110.131821

Imai, Y., K. Kuba, G.G. Neely, R. Yaghubian-Malhami, T. Perkmann, G. van Loo, M. Ermolaeva, R. Veldhuizen, Y.H. Leung, H. Wang, et al. 2008. Identification of oxidative stress and Toll-like receptor 4 signaling as a key pathway of acute lung injury. *Cell.* 133:235–249. http://dx.doi.org/10.1016/j.cell.2008.02.043

Kalinski, P. 2012. Regulation of immune responses by prostaglandin E2. *J. Immunol.* 188:21–28. http://dx.doi.org/10.4049/jimmunol.1101029

Knoops, K., M. Kikkert, S.H. Worm, J.C. Zevenhoven-Dobbe, Y. van der Meer, A.J. Koster, A.M. Mommaas, and E.J. Snijder. 2008. SARS-coronavirus replication is supported by a reticulovesicular network of modified endoplasmic reticulum. *PLoS Biol.* 6:e226. http://dx.doi.org/10.1371/journal.pbio.0060226

Kratzer, E., Y. Tian, N. Sarich, T. Wu, A. Meliton, A. Leff, and A.A. Birukova. 2012. Oxidative stress contributes to lung injury and barrier dysfunction via microtubule destabilization. *Am. J. Respir. Cell Mol. Biol.* 47:688–697. http://dx.doi.org/10.1165/rcmb.2012-0161OC

Kunikata, T., H. Yamane, E. Segi, T. Matsuoka, Y. Sugimoto, S. Tanaka, H. Tanaka, H. Nagai, A. Ichikawa, and S. Narumiya. 2005. Suppression of allergic inflammation by the prostaglandin E receptor subtype EP3. *Nat. Immunol.* 6:524–531. http://dx.doi.org/10.1038/ni1188

Lee, W.M., and P. Ahlquist. 2003. Membrane synthesis, specific lipid requirements, and localized lipid composition changes associated with a positive-strand RNA virus RNA replication protein. *J. Virol.* 77:12819–12828. http://dx.doi.org/10.1128/JVI.77.23.12819-12828.2003

Legge, K.L., and T.J. Braciale. 2005. Lymph node dendritic cells control CD8+ T cell responses through regulated FasL expression. *Immunity.* 23:649–659. http://dx.doi.org/10.1016/j.immuni.2005.11.006

Liu, T., T.M. Laidlaw, C. Feng, W. Xing, S. Shen, G.L. Milne, and J.A. Boyce. 2012. Prostaglandin E2 deficiency uncovers a dominant role for thromboxane A2 in house dust mite-induced allergic pulmonary inflammation. *Proc. Natl. Acad. Sci. USA.* 109:12692–12697. http://dx.doi.org/10.1073/pnas.1207816109

Lorizate, M., and H.G. Kräusslich. 2011. Role of lipids in virus replication. *Cold Spring Harb. Perspect. Biol.* 3:a004820. http://dx.doi.org/10.1101/cshperspect.a004820

MacNee, W. 2011. Aging, inflammation, and emphysema. *Am. J. Respir. Crit. Care Med.* 184:1327–1329. http://dx.doi.org/10.1164/rccm.201110-1764ED

Maitra, U., H. Deng, T. Glaros, B. Baker, D.G. Capelluto, Z. Li, and L. Li. 2012. Molecular mechanisms responsible for the selective and low-grade induction of proinflammatory mediators in murine macrophages by lipopolysaccharide. *J. Immunol.* 189:1014–1023. http://dx.doi.org/10.4049/jimmunol.1200857

Miki, Y., K. Yamamoto, Y. Taketomi, H. Sato, K. Shimo, T. Kobayashi, Y. Ishikawa, T. Ishii, H. Nakanishi, K. Ikeda, et al. 2013. Lymphoid tissue phospholipase A2 group IID resolves contact hypersensitivity by driving antiinflammatory lipid mediators. *J. Exp. Med.* 210:1217–1234. http://dx.doi.org/10.1084/jem.20121887

Miller, S., and J. Krijnse-Locker. 2008. Modification of intracellular membrane structures for virus replication. *Nat. Rev. Microbiol.* 6:363–374. http://dx.doi.org/10.1038/nrmicro1890

Murata, T., K. Aritake, Y. Tsubosaka, T. Maruyama, T. Nakagawa, M. Hori, H. Hirai, M. Nakamura, S. Narumiya, Y. Urade, and H. Ozaki. 2013. Anti-inflammatory role of PGD2 in acute lung inflammation and therapeutic application of its signal enhancement. *Proc. Natl. Acad. Sci. USA.* 110:5205–5210. http://dx.doi.org/10.1073/pnas.1218091110

Nagao, K., H. Tanaka, M. Komai, T. Masuda, S. Narumiya, and H. Nagai. 2003. Role of prostaglandin I2 in airway remodeling induced by repeated allergen challenge in mice. *Am. J. Respir. Cell Mol. Biol.* 29:314–320. http://dx.doi.org/10.1165/rcmb.2003-0035OC

Nagata, N., N. Iwata, H. Hasegawa, S. Fukushi, A. Harashima, Y. Sato, M. Saijo, F. Taguchi, S. Morikawa, and T. Sata. 2008. Mouse-passaged severe acute respiratory syndrome-associated coronavirus leads to lethal pulmonary edema and diffuse alveolar damage in adult but not young mice. *Am. J. Pathol.* 172:1625–1637. http://dx.doi.org/10.2353/ajpath.2008.071060

Nicholls, J.M., L.L. Poon, K.C. Lee, W.F. Ng, S.T. Lai, C.Y. Leung, C.M. Chu, P.K. Hui, K.L. Mak, W. Lim, et al. 2003. Lung pathology of fatal severe acute respiratory syndrome. *Lancet.* 361:1773–1778. http://dx.doi.org/10.1016/S0140-6736(03)13413-7

Novoa, R.R., G. Calderita, R. Arranz, J. Fontana, H. Granzow, and C. Risco. 2005. Virus factories: associations of cell organelles for viral replication and morphogenesis. *Biol. Cell.* 97:147–172. http://dx.doi.org/10.1042/BC20040058

Oslund, R.C., N. Cermak, and M.H. Gelb. 2008. Highly specific and broadly potent inhibitors of mammalian secreted phospholipases A2. *J. Med. Chem.* 51:4708–4714. http://dx.doi.org/10.1021/jm800422v

Peiris, J.S.M., Y. Guan, and K.Y. Yuen. 2004. Severe acute respiratory syndrome. *Nat. Med.* 10:S88–S97. http://dx.doi.org/10.1038/nm1143

Rogerio, A.P., O. Haworth, R. Croze, S.F. Oh, M. Uddin, T. Carlo, M.A. Pfeffer, R. Priluck, C.N. Serhan, and B.D. Levy. 2012. Resolvin D1 and aspirin-triggered resolvin D1 promote resolution of allergic airways responses. *J. Immunol.* 189:1983–1991. http://dx.doi.org/10.4049/jimmunol.1101665

Rossi, A., P. Kapahi, G. Natoli, T. Takahashi, Y. Chen, M. Karin, and M.G. Santoro. 2000. Anti-inflammatory cyclopentenone prostaglandins are direct inhibitors of IkappaB kinase. *Nature.* 403:103–108. http://dx.doi.org/10.1038/47520

Saad, M., A.S. Omrani, K. Baig, A. Bahloul, F. Elzein, M.A. Matin, M.A. Selim, M. Al Mutairi, D. Al Nakhli, A.Y. Al Aidaroos, et al. 2014. Clinical aspects and outcomes of 70 patients with Middle East respiratory syndrome coronavirus infection: a single-center experience in Saudi Arabia. *Int. J. Infect. Dis.* 29:301–306. http://dx.doi.org/10.1016/j.ijid.2014.09.003

Samuelsson, B., S.-E. Dahlén, J.A. Lindgren, C.A. Rouzer, and C.N. Serhan. 1987. Leukotrienes and lipoxins: structures, biosynthesis, and biological effects. *Science.* 237:1171–1176. http://dx.doi.org/10.1126/science.2820055

Serhan, C.N. 2014. Pro-resolving lipid mediators are leads for resolution physiology. *Nature.* 510:92–101. http://dx.doi.org/10.1038/nature13479

Serhan, C.N., S. Hong, K. Gronert, S.P. Colgan, P.R. Devchand, G. Mirick, and R.-L. Moussignac. 2002. Resolvins: a family of bioactive products of omega-3 fatty acid transformation circuits initiated by aspirin treatment that counter proinflammation signals. *J. Exp. Med.* 196:1025–1037. http://dx.doi.org/10.1084/jem.20020760

Smits, S.L., A. de Lang, J.M. van den Brand, L.M. Leijten, W.F. van IJcken, M.J. Eijkemans, G. van Amerongen, T. Kuiken, A.C. Andeweg, A.D. Osterhaus, and B.L. Haagmans. 2010. Exacerbated innate host response to SARS-CoV in aged non-human primates. *PLoS Pathog.* 6:e1000756. http://dx.doi.org/10.1371/journal.ppat.1000756

Straus, D.S., G. Pascual, M. Li, J.S. Welch, M. Ricote, C.-H. Hsiang, L.L. Sengchanthalangsy, G. Ghosh, and C.K. Glass. 2000. 15-deoxy-delta 12,14-prostaglandin J2 inhibits multiple steps in the NF-κ B signaling pathway. *Proc. Natl. Acad. Sci. USA.* 97:4844–4849. http://dx.doi.org/10.1073/pnas.97.9.4844

Sun, G.Y., J. Xu, M.D. Jensen, and A. Simonyi. 2004. Phospholipase A2 in the central nervous system: implications for neurodegenerative diseases. *J. Lipid Res.* 45:205–213. http://dx.doi.org/10.1194/jlr.R300016-JLR200

Vancheri, C., C. Mastruzzo, M.A. Sortino, and N. Crimi. 2004. The lung as a privileged site for the beneficial actions of PGE2. *Trends Immunol.* 25:40–46. http://dx.doi.org/10.1016/j.it.2003.11.001

von Allmen, C.E., N. Schmitz, M. Bauer, H.J. Hinton, M.O. Kurrer, R.B. Buser, M. Gwerder, S. Muntwiler, T. Sparwasser, R.R. Beerli, and M.F. Bachmann. 2009. Secretory phospholipase A2-IID is an effector molecule of CD4+CD25+ regulatory T cells. *Proc. Natl. Acad. Sci. USA.* 106:11673–11678. http://dx.doi.org/10.1073/pnas.0812569106

Xu, K., and P.D. Nagy. 2015. RNA virus replication depends on enrichment of phosphatidylethanolamine at replication sites in subcellular membranes. *Proc. Natl. Acad. Sci. USA.* 112:E1782–E1791. http://dx.doi.org/10.1073/pnas.1418971112

Zhao, J., J. Zhao, N. Van Rooijen, and S. Perlman. 2009. Evasion by stealth: inefficient immune activation underlies poor T cell response and severe disease in SARS-CoV-infected mice. *PLoS Pathog.* 5:e1000636. http://dx.doi.org/10.1371/journal.ppat.1000636

Zhao, J., J. Zhao, K. Legge, and S. Perlman. 2011. Age-related increases in PGD(2) expression impair respiratory DC migration, resulting in diminished T cell responses upon respiratory virus infection in mice. *J. Clin. Invest.* 121:4921–4930. http://dx.doi.org/10.1172/JCI59777

Zhao, J., C. Wohlford-Lenane, J. Zhao, E. Fleming, T.E. Lane, P.B. McCray Jr., and S. Perlman. 2012. Intranasal treatment with poly(I•C) protects aged mice from lethal respiratory virus infections. *J. Virol.* 86:11416–11424. http://dx.doi.org/10.1128/JVI.01410-12